RECLAMATION
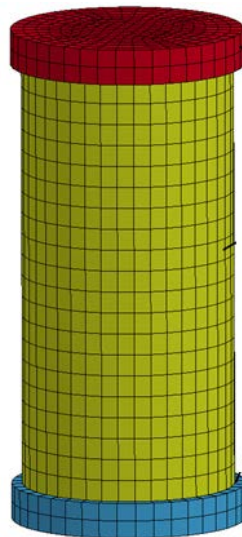### *Managing Water in the West*

Report DSO-2014-08

Evaluation of Nonlinear Material Models in Concrete Dam Finite Element Analysis

Dam Safety Technology Development Program

The public reporting burden for this collection of information is estimated to average 1 hour per response, including the time for reviewing instructions, searching existing data sources, gathering and maintaining the data needed, and completing and reviewing the collection of information. Send comments regarding this burden estimate or any other aspect of this collection of information, including suggestions for reducing the burden, to Department of Defense, Washington Headquarters Services, Directorate for Information Operations and Reports (0704-0188), 1215 Jefferson Davis Highway, Suite 1204, Arlington, VA 22202-4302. Respondents should be aware that notwithstanding any other provision of law, no person shall be subject to any penalty for failing to comply with a collection of information if it does not display a currently valid OMB control number.
PLEASE DO NOT RETURN YOUR FORM TO THE ABOVE ADDRESS.

1. REPORT DATE *(September 2014)* September 2014	2. REPORT TYPE Final	3. DATES COVERED *(From - To)*

4. TITLE AND SUBTITLE Evaluation of Nonlinear Material Models in Concrete Dam Finite Element Analysis	5a. CONTRACT NUMBER
	5b. GRANT NUMBER
	5c. PROGRAM ELEMENT NUMBER
6. AUTHOR(S) Jerzy Salamon, Ph.D., P.E., Denver, Colorado, D-86-68110 David W. Harris, Ph.D., P.E., Consultant	5d. PROJECT NUMBER
	5e. TASK NUMBER
	5f. WORK UNIT NUMBER

7. PERFORMING ORGANIZATION NAME(S) AND ADDRESS(ES) Bureau of Reclamation, Denver Federal Center, P.O. Box 25007, Denver, CO, 80225	8. PERFORMING ORGANIZATION REPORT NUMBER

9. SPONSORING/MONITORING AGENCY NAME(S) AND ADDRESS(ES) Bureau of Reclamation, Denver Federal Center, P.O. Box 25007, Denver, CO, 80225	10. SPONSOR/MONITOR'S ACRONYM(S)
	11. SPONSOR/MONITOR'S REPORT NUMBER(S)

12. DISTRIBUTION/AVAILABILITY STATEMENT

13. SUPPLEMENTARY NOTE

14. ABSTRACT
This report presents a study performed to validate a new concrete constitutive material model implemented in LS-DYNA Finite Element program by ADAPTEC in 2007 for concrete dam applications. The new Continues Surface Cap Model (CSCM) was successfully used by Federal Highway Administration for the highway related projects. The main objective of this study are to evaluate the effectiveness of the CSCM in the nonlinear analysis of concrete dams and to calibrate the input parameters of CSCM against the data obtained from laboratory test.

15. SUBJECT TERMS
Reclamation, nonlinear material models, concrete material models, Finite Element Method

16. SECURITY CLASSIFICATION OF:			17. LIMITATION OF ABSTRACT	18. NUMBER OF PAGES	19a. NAME OF RESPONSIBLE PERSON Jerzy Salamon
a. REPORT U	b. ABSTRACT U	a. THIS PAGE U		89	19b. TELEPHONE NUMBER *(Include area code)* 303-445-3219

Standard Form 298 (Rev. 8/98)
Prescribed by ANSI Std. Z39.18

Report DSO-2014-08

Evaluation of Nonlinear Material Models in Concrete Dam Finite Element Analysis

Dam Safety Technology Development Program

Prepared by:

Jerzy Salamon, Ph.D., P.E.
David W. Harris, Ph.D., P.E.

MISSION STATEMENTS

The U.S. Department of the Interior protects America's natural resources and heritage, honors our cultures and tribal communities, and supplies the energy to power our future.

The mission of the Bureau of Reclamation is to manage, develop, and protect water and related resources in an environmentally and economically sound manner in the interest of the American public.

BUREAU OF RECLAMATION
Dam Safety Technology Development Program
Structural Analysis Group, 86-68110

DSO-2014-08

Evaluation of Nonlinear Material Models in Concrete Dam Finite Element Analysis

Author: Sections 1, 4 to 8 and Checking: Sections 2 and 3:
Jerzy Salamon, Ph.D., P.E., Structural Analysis, 86-68110

Author: Sections 2 and 3 and Checking: Sections 1, 4 to 8:
David W. Harris, Ph.D., P.E., Consultant

Peer Review: Veronica Madera, P.E.   11/13/14
Materials Engineering & Research Laboratory, 86-68180   Date

Technical Approval: Jerzy Salamon, Ph.D., P.E.   11/17/14
Structural Engineer, Structural Analysis, 86-68110   Date

<table>
<tr><td colspan="6" align="center">REVISIONS</td></tr>
<tr><td>Date</td><td>Description</td><td>Prepared</td><td>Checked</td><td>Technical approval</td><td>Peer review</td></tr>
<tr><td></td><td></td><td></td><td></td><td></td><td></td></tr>
<tr><td></td><td></td><td></td><td></td><td></td><td></td></tr>
<tr><td></td><td></td><td></td><td></td><td></td><td></td></tr>
</table>

ACRONYMS AND ABBREVIATIONS

ACI	American Concrete Institute
ASTM	American Society for Testing and Materials
CEB	Comité Euro-International du Béton
CSCM	Continuous Surface Cap Model
DIF	dynamic increase factor
EOS	Equation of State
FE	finite element
KCC	Karagozian Case Concrete
lbf	Pound Force Pascal
MPa	Mega Pascal
NMSA	nominal maximum size aggregate
psi	pounds per square inch
Reclamation	Bureau of Reclamation
TOR	triaxial torsion
TSC	Technical Service Center
TXE	triaxial extension
TXC	triaxial compression
USBR	Bureau of Reclamation
UUC	unconfined uniaxial compression
UUT	unconfined uniaxial tension
UXC	uniaxial compression
w/c	water to cement ratio
w/cm	water to cementitious material ratio
WSMR	White Sands Missile Range

Symbols

°F	degrees Fahrenheit
%	percent

CONTENTS

Tables

Figures

Attachments

Attachment

A	Detailed Data for Black Canyon Dam
B	Continuous Surface Cap Model Input Parameters

1.0 GENERAL

1.1 Introduction

In structural evaluations of the Bureau of Reclamation's (Reclamation) concrete dams, complex analyses are performed for hydrostatic, thermal, and seismic loads. The finite element (FE) method based LS-DYNA commercial software used by the Technical Service Center's (TSC) Structural Analysis Group has an extensive built-in library of material models, some of which can represent a vast range of concrete behavior, but also exhibit certain limitations in modeling the real concrete performance.

An investigation performed by the TSC in 2006 reported features of material models within the DYNA series. Two constitutive models, the Concrete/ Geological Model (Mat 16 - *MAT_PSEUDO_TENSOR) and the Karagozian & Case Concrete Model (MAT_72 or *MAT_CONCRETE_DAMAGE), are described in some detail (Reclamation 2006).

In this report, we summarize a study performed to validate new concrete constitutive material models implemented more recently in LS-DYNA code. The investigation included two concrete models:

- Continuous Surface Cap Model (CSCM) (*Mat_159 or MAT_CSCM) implemented by Adaptec (2007) for Federal Highway Administration applications

- Karagozian & Case Concrete Model, Release III (*MAT_072R3 or *MAT_CONCRETE_DAMAGE_REL3), hereafter referred to as the KCC model, with significant changes implemented to its previous *MAT_72 version.

1.2 Objectives and Scope of Work

The main objectives of this investigation, funded under the Dam Safety Research Program, are to:

- Evaluate the effectiveness of the CSCM and KCC models in nonlinear analysis of concrete dams

- Calibrate the input parameters of CSCM and the KCC model against results obtained from laboratory tests

- Perform a comparison analysis between the CSCM and the new KCC model

- Summarize the analysis results and derive conclusions on the effectiveness of the CSCM for application to the nonlinear analysis of concrete dams

The results of this research would allow use of these more enhanced material models in the nonlinear analysis of concrete dams for static and earthquake loads.

2.0 PROPERTIES OF CONCRETE FOR DAMS

Mass concrete is defined by American Concrete Institute (ACI) Committee 207 as "*any volume of concrete with dimensions large enough to require that measures be taken to cope with the generation of heat from hydration of cement and attendant volume change to minimize cracking*" [ACI-207)].

Properties of concrete for dams are heavily influenced by the:

- Cement and other cementitious materials chemistry
- Water to cementitious material (w/cm) ratio
- Age of the dam
- Aggregate size
- Construction methods
- Environment of the dam
- State of the practice within the era of placement for the concrete

2.1 Immediate and Long-Term Influences on Mechanical Properties

The factors influencing improvements in conventional concrete dams were highlighted by Dolen (2010) and are shown on figure 2.1 in a timeline. Much of this state of the practice discussion by Dolen is in this section to aid in identifying the differences in behavior between conventional concrete for dams and conventional concrete for typical structures.

The relationship between the water to cement (w/c) ratio and strength was developed by Abrams (1918). This "law" states that concrete strength generally increases as the w/c ratio decreases. This property is assumed to apply for all types of concrete.

The design and construction of Hoover and Grand Coulee Dams in the 1930s led to the development of concrete production on a massive scale, including improvements in concrete mixing, transporting, placing, and cooling. Close control of concrete quality led to reductions in the water and cement contents, yielding greater economy and more volumetric stability.

The development of cement chemistry was spurred on in the late 1920s by the need to understand the chemical processes of hydration in order to reduce cracking from thermal heat generation for large dams and in particular Hoover Dam. Low-heat cements were originally developed for Hoover Dam mass concrete and subsequently improved and used in future dams.
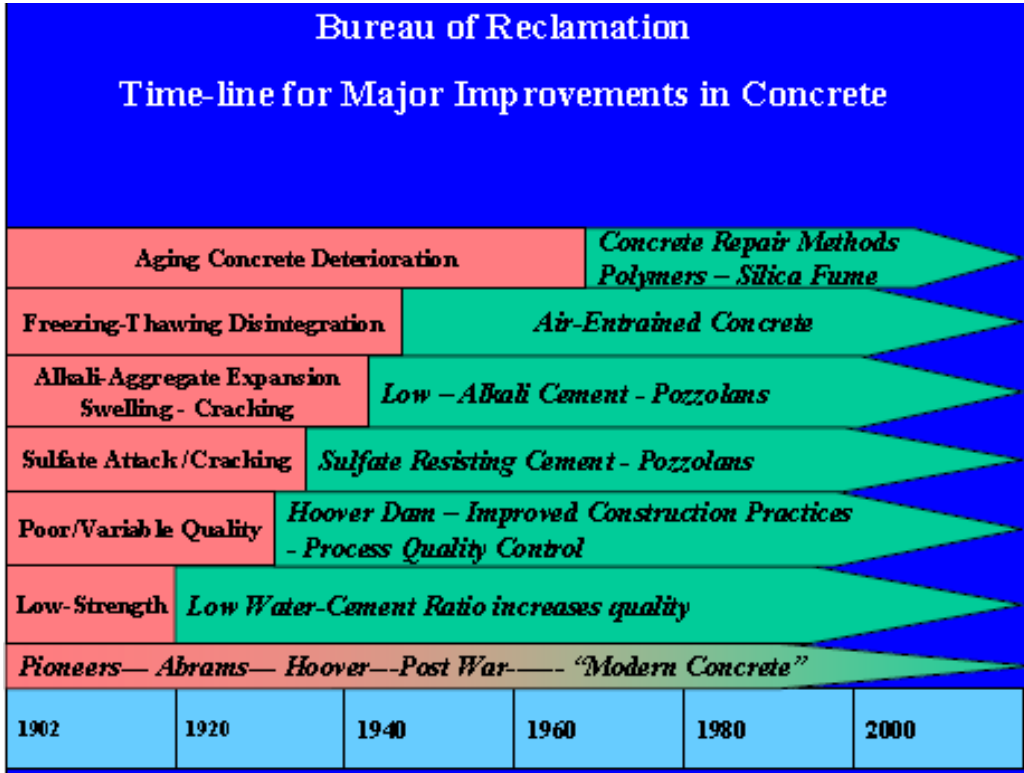
Figure 2.1.—A timeline for Reclamation aging concrete (Dolen, 2010).

Pozzolans are used primarily as a partial replacement for Portland cement to reduce the heat of hydration. Most fly ashes have the ability to improve the workability of concrete and reduce the water content by 5 to 8 percent (%).

Mass concrete is referred to as such due to the nature of the concrete and its placement and requires considerations for heat generation. When proportioning concrete for dams, the nominal maximum size aggregate (NMSA) determines to a large degree the cement content of the mixture. Increasing the NMSA decreases the void space between the largest through the smallest particles and thus reduces the volume of voids that must be filled with cement paste. The lowest volume of cement paste reduces the internal heat of hydration that must be expelled and reduces the overall cost of the concrete due to less cement. The largest practical NMSA is based not only on what is available in local borrow areas, but also on the ability to effectively mix, transport, and place the concrete. Early Reclamation dams used either quarried stone blocks or embedded "plum stones," up to 3 or 4 feet in diameter, surrounded by 1- to 4-inch NMSA mixtures. These dams had high dimensional stability due to the high aggregate volume.

Early concrete dam mix design resulted in air void contents of 1–2% by volume. As discussed by Dolen in the history of concrete mix design, air entrainment additives would be investigated and utilized with mixes starting approximately after the Second World War. The use of air entrainment agents increases the air

void ratio to a level more consistent with modern conventional concretes, 4–7%. Void space may be small in older dams due to a low air void at placement and a level of saturation over time.

When large (mass) sections are formed, cracking due to temperature rise may be a concern after the initial volumetric expansion and later contraction. In the first stages of mass concrete life, about the first year of age, heat is generated from the exothermic chemical reaction of cement hydration. However, concrete and aggregates have very little capacity to expel the heat, which then builds up in the dam. Without measures to mitigate these reactions, the interior temperature rises to 125 to 150 degrees Fahrenheit (°F), creating initial expansion of the structure and producing a temperature gradient between the cooling exterior surface and the heating interior mass. Long-term thermal contraction of the dam would be on the order of about 6 inches over decades. In addition, if the temperature gradient exceeds about 35 °F, unreinforced mass concrete is likely to crack. These cracks must be controlled to avoid structural damage, leakage, and durability concerns.

To assure monolithic behavior in a dam, special preparation methods are utilized to establish strength on lift lines and the intermediate horizontal joints between subsequent mass concrete placements. Studies were conducted at the engineering and materials laboratories of the University of California at Berkley under the direction of Professor Raymond E. Davis (Davis et al., 1932). Hoover Dam specifications required a 72-hour delay between each 5-foot-high placement and that the difference in height between adjacent blocks should not exceed 35 feet in height (Reclamation, 1949). Preparation of the lift surface before resuming mass concrete placement was primarily accomplished by scarifying the lift surface after appropriate time delays. The typical lift line was cleaned by pressurized air-water jetting and timed to remove the surface layer of cement paste to expose aggregates.

The low-heat cements originally developed for Hoover Dam mass concrete also were found to resist deterioration in a sulfate environment. Subsequently, this materials science methodology became the foundation for the investigations in durability of concrete to resist sulfate attack, alkali-aggregate reaction, and freezing and thawing deterioration. These improvements are used in all concrete types. Trends of concrete materials properties have been developed for these different generations of concrete dam construction. Some dams have exceeded their expectations, while others have not.

Comparing these concretes and their environment and exposure conditions proved beneficial to discoveries of the necessary properties for durable concrete. Exposed concrete at Arrowrock Dam in Idaho and Lahontan Dam in California required significant repair within 20 years and ultimately total rehabilitation of the service spillways, whereas similar concrete used at Elephant Butte Dam in New Mexico was, for the most part, unaffected. The mixtures for Hoover and Grand Coulee Dams have proved superior in their respective environments

compared to almost identical concretes constructed at the other locations with alkali-reactive siliceous aggregates. Results estimating the properties as a function of age for Grand Coulee, Hoover, and Parker Dams are shown on figure 2.2 (Dolen, 2005).
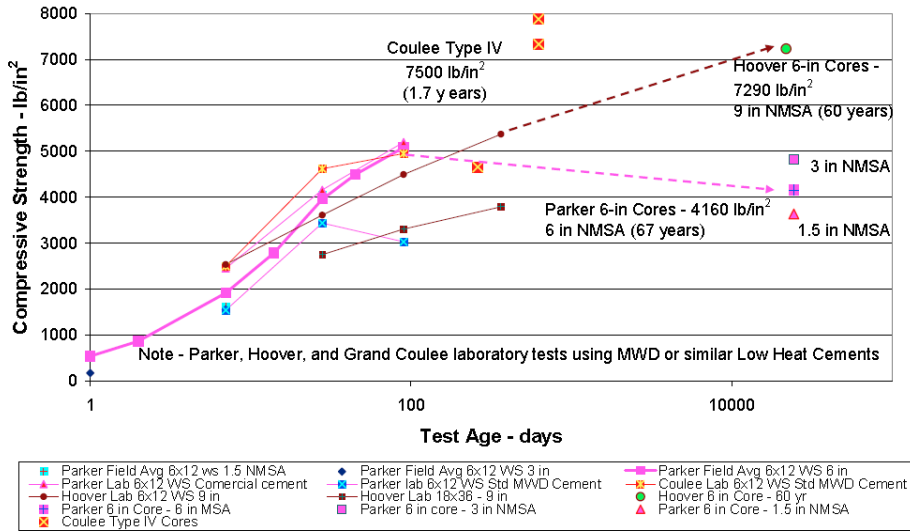
Figure 2 Compressive Strength vs. Age of Laboratory Test Cylinders and Cores – Type IV (Low Heat) Cement – Parker, Grand Coulee, and Hoover Dams.

Figure 2.2.—Age effects for three dams (Dolen, 2005).

Additional details from the abstracted information in this section may be found in the Dolen references.

Differences in the properties of dams, having undergone various influences, make the trends of properties different from conventional structural concrete and, in many cases, different from dam to dam.

2.2　Mechanical Properties Obtained from Laboratory Tests

A conceptual stress-strain curve for uniaxial data from concrete testing is shown on figure 2.3. Of particular interest in this figure is the initial slope of the curve, up to the yield point, which is measured by the Modulus of Elasticity, a linear, elastic parameter. Also note the maximum point, maximum or ultimate strength, measured in the tests and discussed later. With linear analysis, the elastic properties, in this case the modulus, are needed for the formulation of the analysis, and the ultimate strength is used for a comparison to the calculated results to judge the safety of the structure.
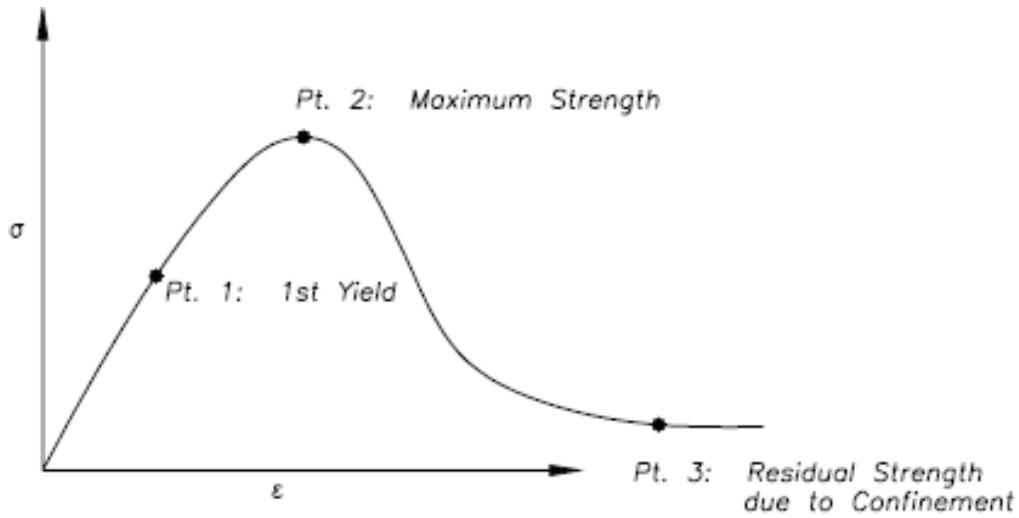
Figure 2.3.—Conceptual phases of concrete uniaxial test results (Malvar et.al., 1994).

Measured values of Modulus of Elasticity for cores removed from various dams are shown on figure 2.4.
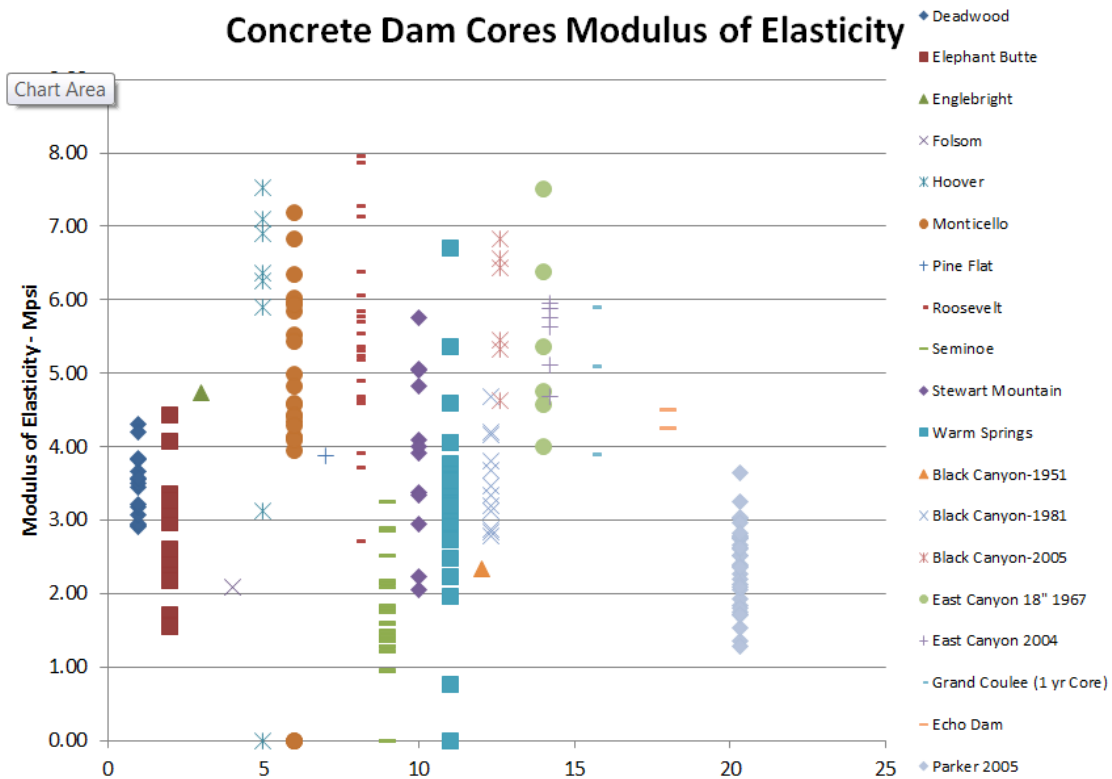
Figure 2.4.—Modulus of Elasticity values measured from dam cores.
(Data compiled by Harris; data courtesy of Materials Engineering and Research Laboratory)

A wide range for tested values of elastic modulus was previously reported (Harris et al., 2000). The columns of data represent multiple tests for a single site. For columns showing a zero value, there was a sample selected for testing that could not be tested. In the overall data, the range of values is from 0.76 to 7.96 x10^6 pounds per square inch (psi) with a median of 3.34. The median of all values appears typical of values suggested for structural design; however, this range is atypical of structural design recommended values. Also notice how Hoover Dam values compare to the similar mix design for Parker Dam, which shows effects with a more reactive aggregate as mentioned above.

Median or average values may not be best for use in the evaluation of dams. Figure 2.5 compares average values and 80% exceedance from values on figure 2.4. The 80% exceedance approach is similar to construction specifications in which 80% of all values are greater than the value given. The notion of being conservative with different modulus values is not as clear as with strength values. This will be discussed later once measured strains can be reviewed. For now, note that for the same stress level, higher strains are computed with linear analysis for lower modulus values.
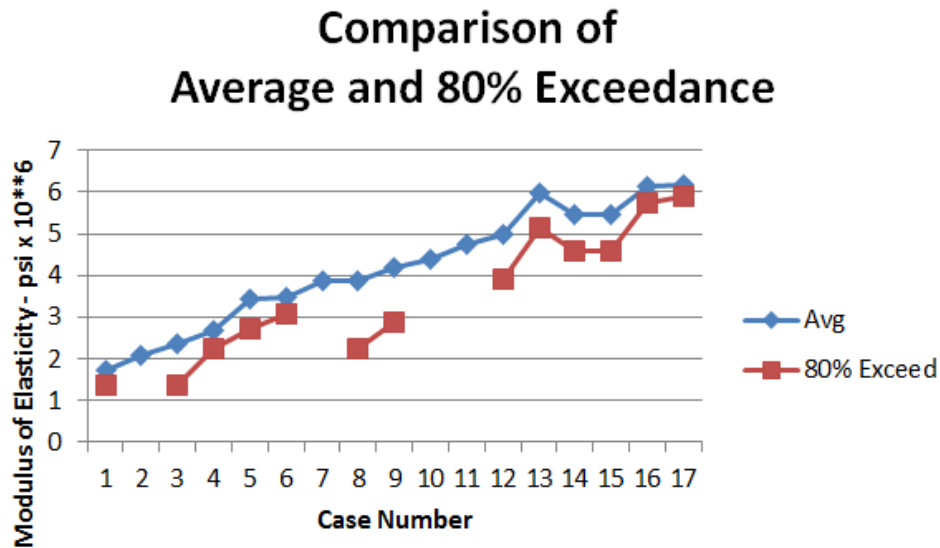
Figure 2.5.—Comparison of Modulus Elasticity average and 80% exceedance. (Data compiled by Harris; data courtesy of Materials Engineering and Research Laboratory)

Figure 2.6 shows measured values for ultimate compressive strength from dam cores. A range of values is also seen in the compressive strength as shown with elastic modulus – the minimum is 1,270 psi, and the maximum is 9,230 psi, with the median being 4,300 psi. As with the elastic modulus, the median of all strength values appears typical to structural design recommendations while the range is atypical.
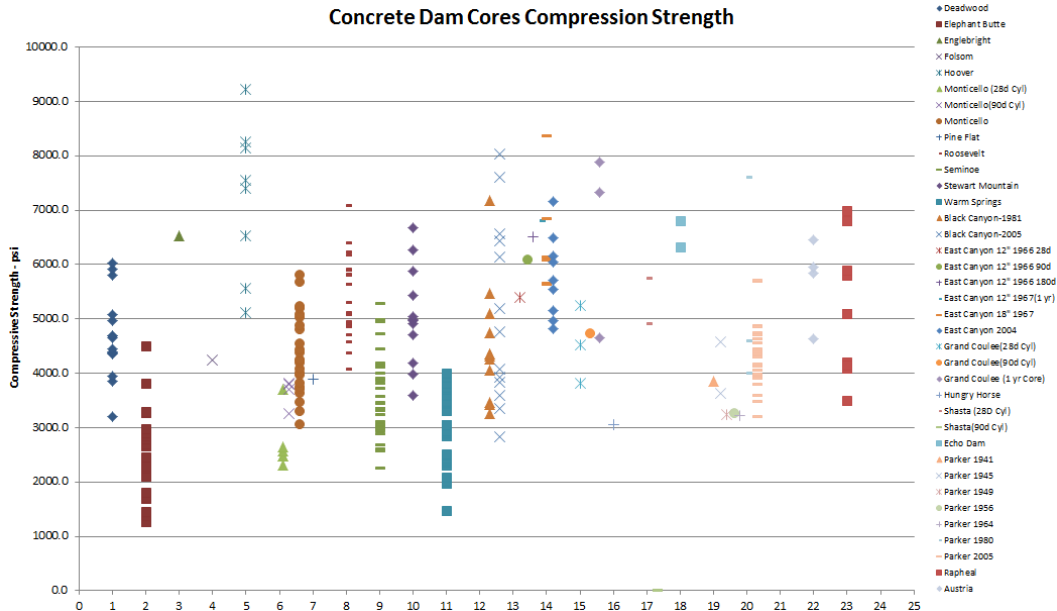
Figure 2.6.—Compression strength measured from dam cores.
(Data compiled by Harris; data courtesy of Materials Engineering and Research
Laboratory)

Figure 2.7 compares the average compressive strength values and the 80%
exceedance. On figure 2.7 (right), as would be expected, average values are
greater than the 80% exceedance values (this owing to the average line being
essentially a 50% exceedance line). The average values are 1.1 to 1.4 times
greater than the 80% exceedance approach. Figure 2.8 also shows the concept of
exceedance with measured values. In this presentation, the relationship to a bell-
type distribution and standard deviation can be observed. The value shown as the
standard deviation is the strength accounting for the standard deviation, not the
actual standard deviation itself. Use of these tools provides methods to compare
analysis results to known measured values.
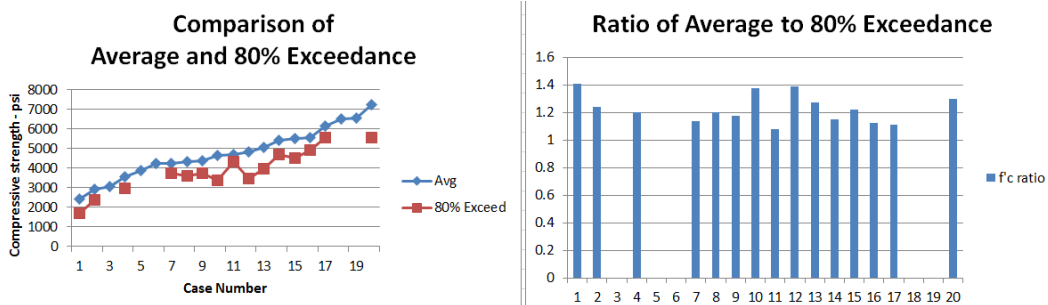
**Figure 2.7.—Comparison of average compressive strength values and 80%
exceedance values.**
(Data compiled by Harris; data courtesy of Materials Engineering and Research
Laboratory)

East Canyon Compression Strength
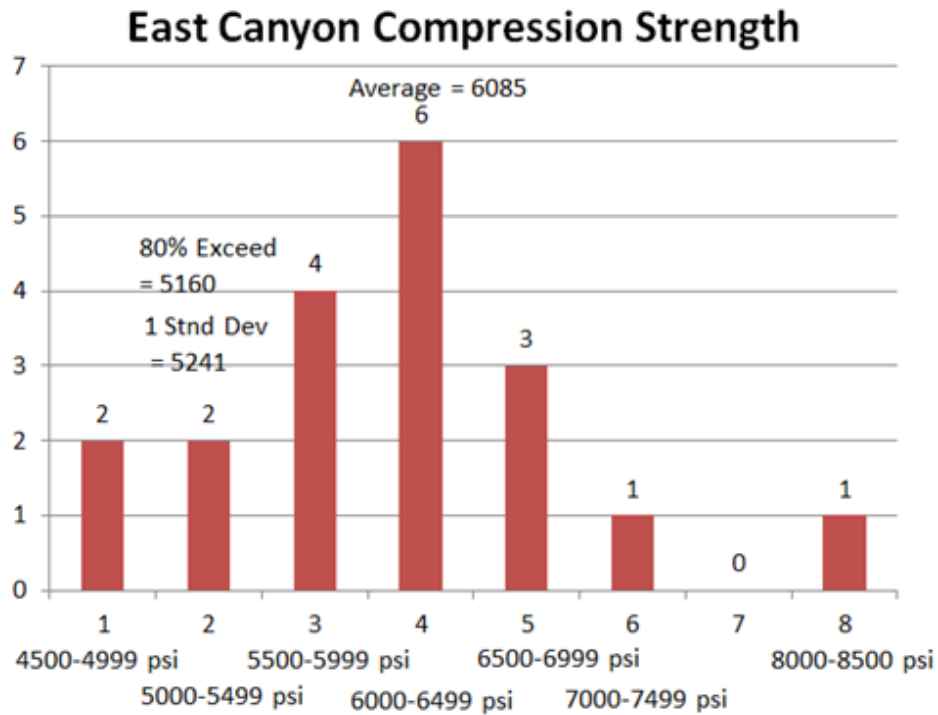
Figure 2.8.—Distribution of measured values for East Canyon Dam.
(Data compiled by Harris; data courtesy of Materials Engineering and Research
Laboratory).

Note that loads used in the analysis of dams are natural values and are not increased by load factors. Thus, the analysis falls within an allowable stress approach (used for conventional structures), and the choice of comparison values needs to be made judiciously. Structural concrete is generally designed with a factored loads approach.

Figure 2.9 shows measured values of strains at ultimate strength. Linear and nonlinear analyses need to be checked to assure that known, measured strains are not exceeded. This provides an additional needed check on safety of the structure. Strain values from cores tested in compression range from 0.0007 to 0.0028 with a median of 0.0015. For these values, the absolute maximum is below the suggested ACI 318 strain value of 0.003 for conventional structure designs, and the median is one-half of this value. This is a major difference between concrete used in conventional structures and cores tested from aged concrete in dams.
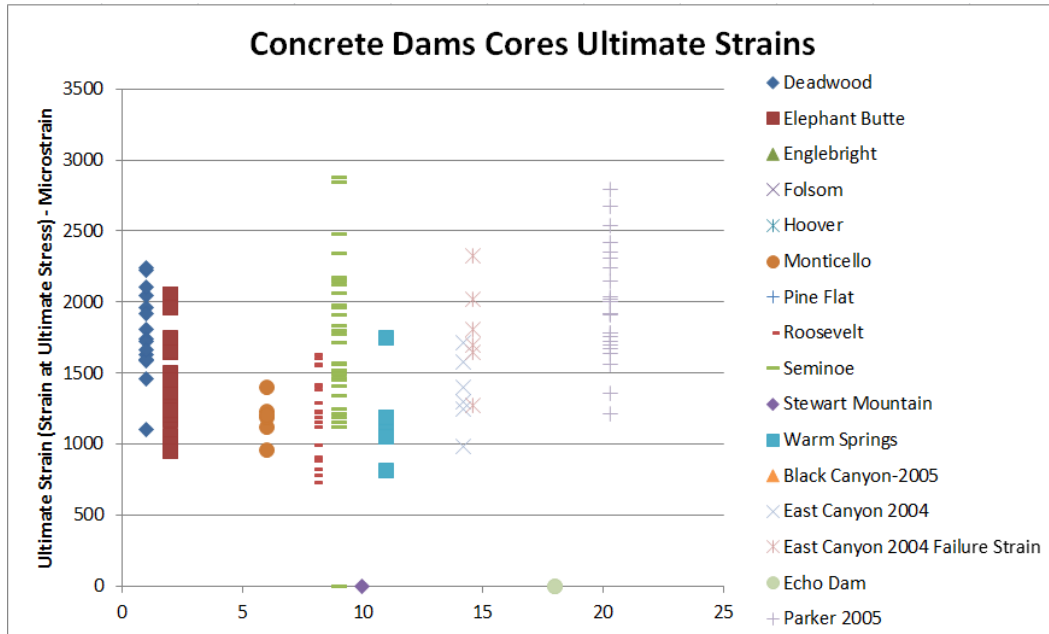
Figure 2.9.—Compressive strain values at ultimate stress for concrete dam cores.
(Data compiled by Harris; data courtesy of Materials Engineering and Research
Laboratory).

Figure 2.10 shows measured direct tensile strength values. As in all previous
cases, a range is seen, but there are not a significant number of values to allow for
an exceedance evaluation. Tensile and compressive strength values will be
compared in the next section.
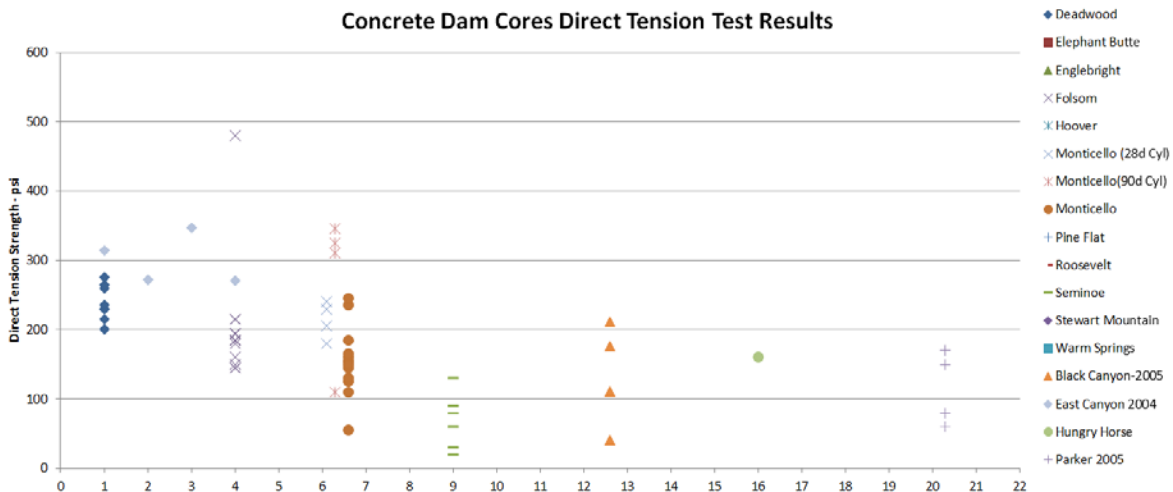
Figure 2.10.—Direct tensile strength of dam cores.
(Data compiled by Harris; data courtesy of Materials Engineering and Research Laboratory)

Figure 2.11 shows values for the American Society for Testing and Materials (ASTM) C496 test to determine the splitting tensile strength of concrete. As in all other cases, there is a range in the values. Use of these values for comparison to analysis results needs to be done with care that the biaxial stress state used in the test is being compared to similar stress conditions in the analysis.
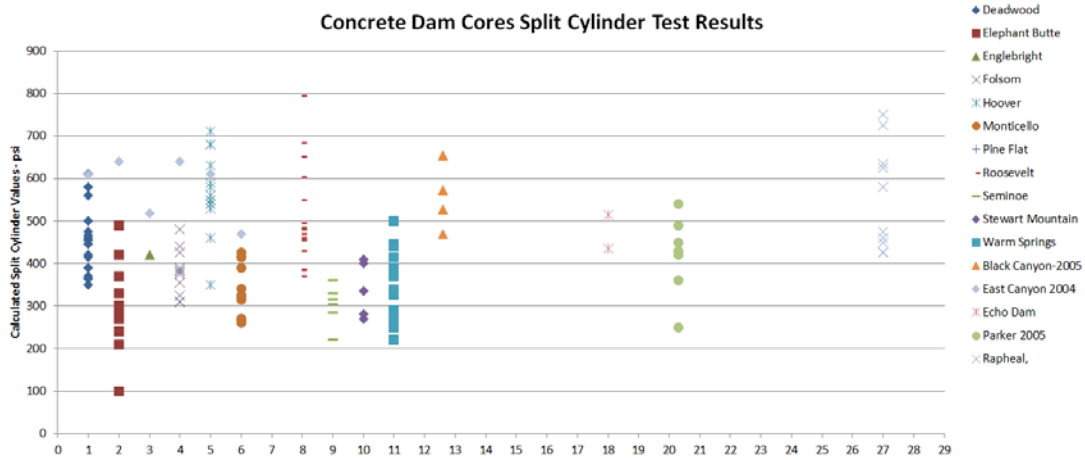
Figure 2.11.—Split cylinder test results from dam cores.
(Data compiled by Harris; data courtesy of Materials Engineering and Research Laboratory)

The compressive strength test, with or without Modulus and Poisson's ratio measurement, and the split cylinder has been executed at higher strain rates on the order of a 10^{-3} strain rate. Measured values of elastic modulus, compressive strength, and splitting test strength are shown on figures 2.12 through 2.14. Projecting dynamic values from static values will be discussed in the following section.

Direct shear and triaxial test results will be presented in the next section in the description of the formulation of stress path surfaces. Stress path surfaces are used in nonlinear material simulations.

2.3   Properties Estimated on the Basis of Other Properties

Uniaxial test data for the ultimate strength of concrete are the most common. Approximations have been suggested to link various properties to the strength. One well known approximation is the ACI-318 (2011) equation for conventional structural concrete to estimate elastic modulus:

$$\text{ACI 318 Estimation: } E = 57000 \ \sqrt{(f'_c)}$$

Concrete Dams Dynamic Compression Modulus
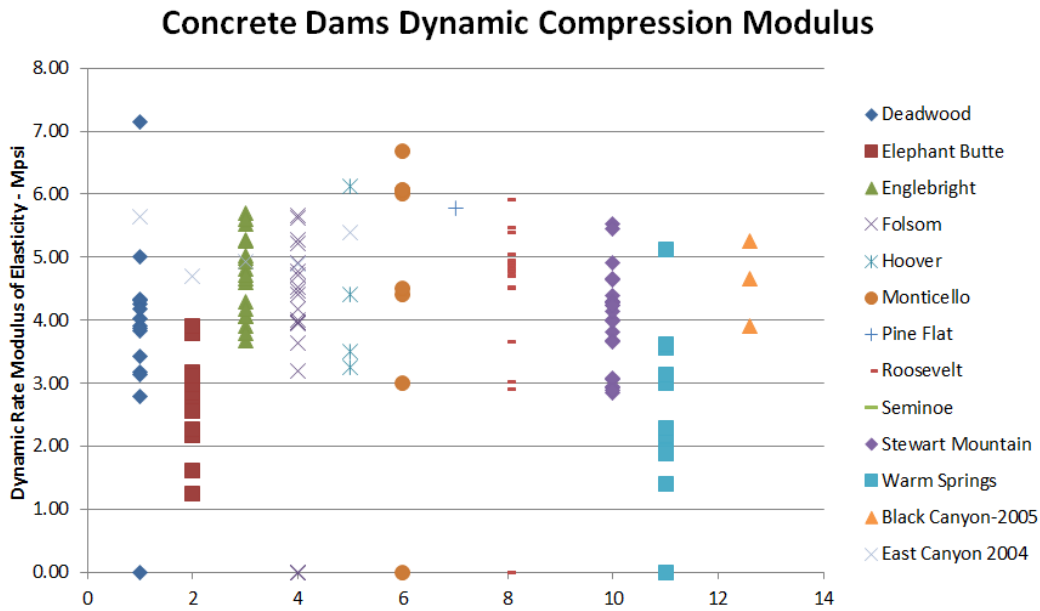
Figure 2.12.—Elastic modulus, in compression, at a 10^{-3} strain rate.
(Data compiled by Harris; data courtesy of Materials Engineering and Research
Laboratory)

Concrete Dams Dynamic Compression
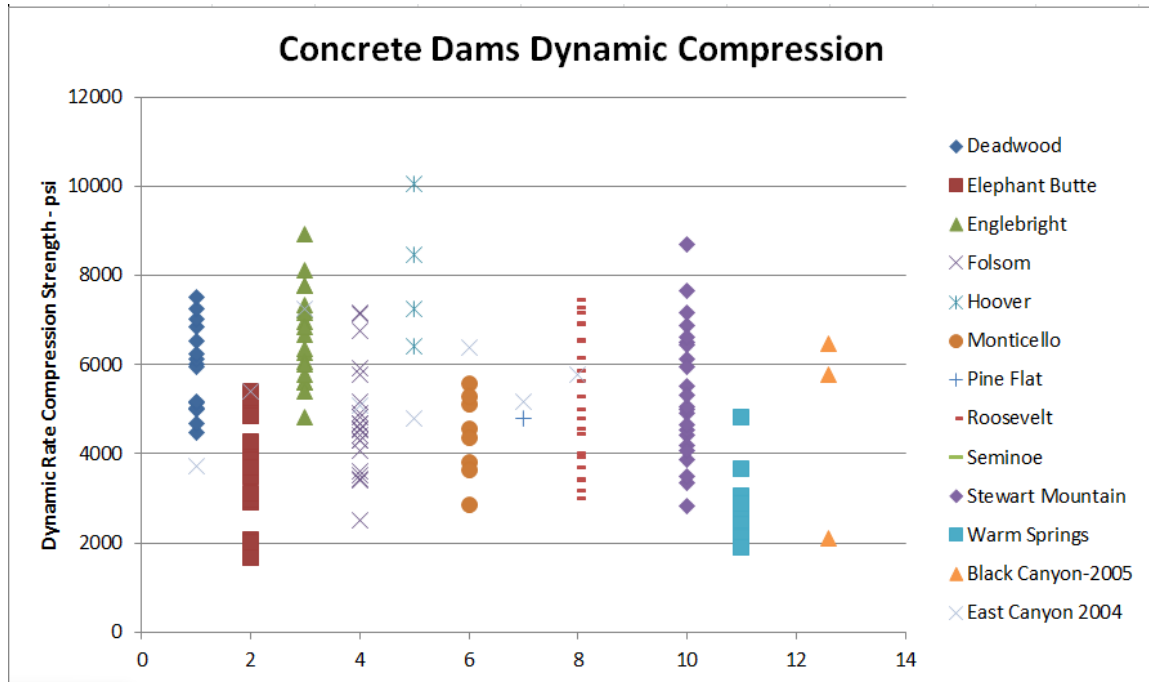
Figure 2.13.—Compressive strength at a 10^{-3} strain rate.
(Data compiled by Harris; data courtesy of Materials Engineering and Research
Laboratory)
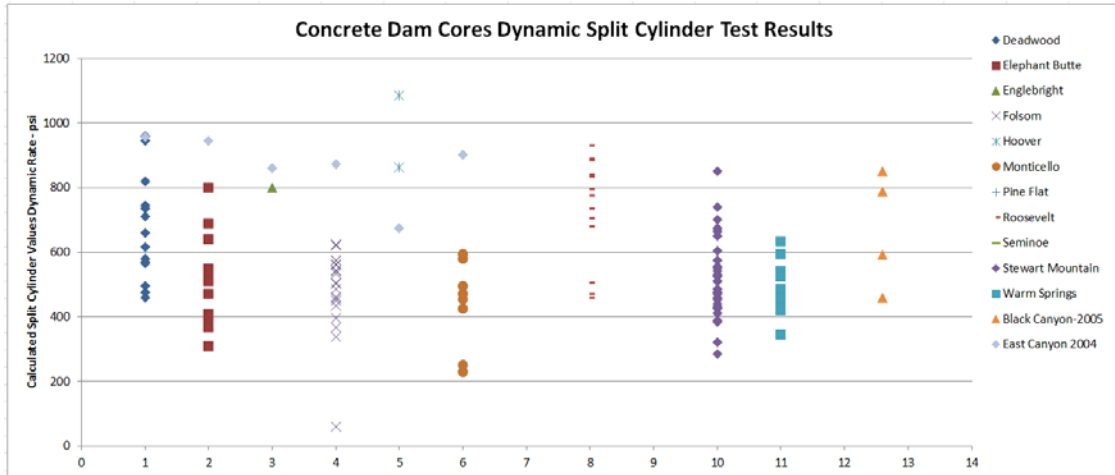
Figure 2.14.—Splitting tensile strength at a 10^{-3} strain rate.
(Data compiled by Harris; data courtesy of Materials Engineering and Research Laboratory)

With another approximation from the Comité Euro-International du Béton (CEB) (1993):

$$\text{CEB approximation } E = E_{ceb} \, (f'_c/10)^{1/3}$$

where f'_c is the concrete compressive strength and E_{ceb} = 18.275 MPa (2,651 psi), which is the value of Young's modulus when $f'c$ = 10 MPa (1,450 psi).

These approximations are shown with measured values of modulus and compressive strength and least squares linear and polynominal fits with the data on figure 2.15. In these comparisons, it can be seen that the ACI and CEB approximations yield low values for higher strengths compared to least squares fits through the data, with the CEB being the lowest.

Figure 2.16 compares measured stress and strain data with high and low values from the CEB approximation. This diagram gives some insight into the effects of the choice of modulus on an analysis. An 80% line, in this case 80% of all strain values are below this line, is shown in the diagram. Note that with lower values of elastic modulus (using linear analysis or during incremental time steps), a fairly large number of the data points lie above the prediction line. Points below the line would be conservative, below the prediction, while points above the line would be nonconservative above the predicted value. Conversely, a higher modulus value forms an envelope of most of the data points. Care must also be taken if lower values of modulus are chosen that maximum failure strains are not overpredicted before a failure stress condition is reached. Thus, in general, higher values of modulus should be given preference when a choice is necessary. As the ACI and CEB estimating methods were derived from data on conventional structural concrete tests and predict lower values than measured in dam cores, these methods need to be used with care and judgment. Linear and
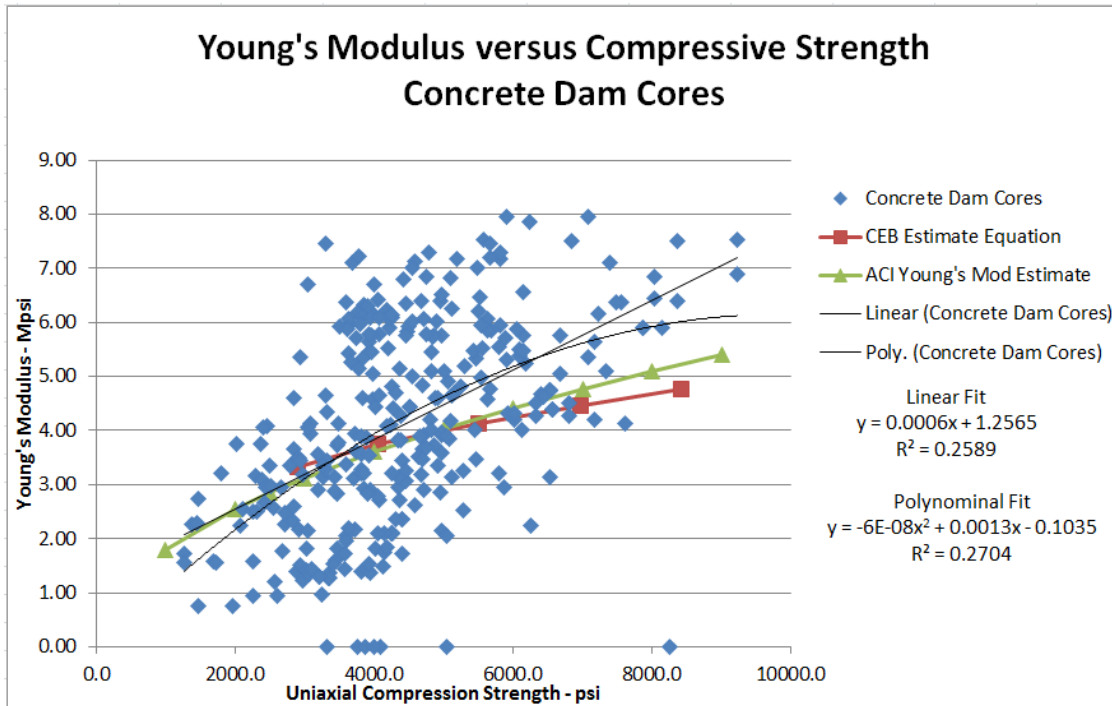
**Figure 2.15.—Measured modulus compared to measured compressive strength and
various estimates.**
(Data compiled by Harris; data courtesy of Materials Engineering and Research Laboratory)
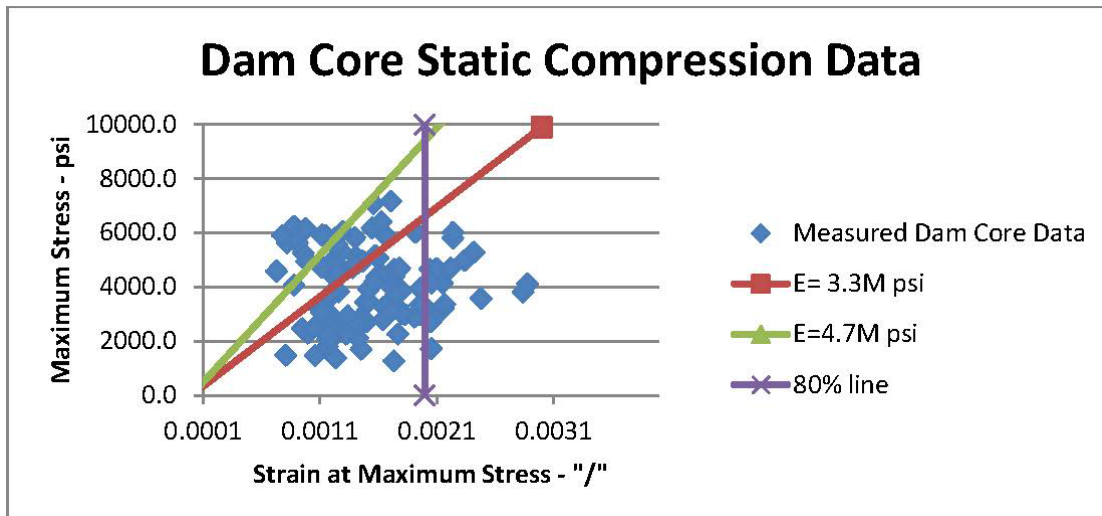
**Figure 2.16.—Stress-strain data from dam cores compared to calculated modulus
values.**
(Data compiled by Harris; data courtesy of Materials Engineering and Research Laboratory)

polynomial fits to the data are also not particularly good fits. Elastic modulus values used for analysis of critical structures are best found using site-specific data.

Another prediction based on compressive strength has been suggested for tensile strength. Tensile properties of concrete in dams show lower values from what is typically expected for conventional concrete. Figure 2.17 compares direct tensile and compressive strength data. As can be seen in this figure, the best linear fit shows a ratio of tension to compression of 4.5%. Note that the correlation constant, R^2, for this fit is poor, with a value of 0.08, which is due to large scatter in the data that does not fit a straight line. A rule of thumb for the tension to compression ratio with conventional concrete is 10%, but note this is based on comparison to the split cylinder values, which are known to be higher than direct tension values.
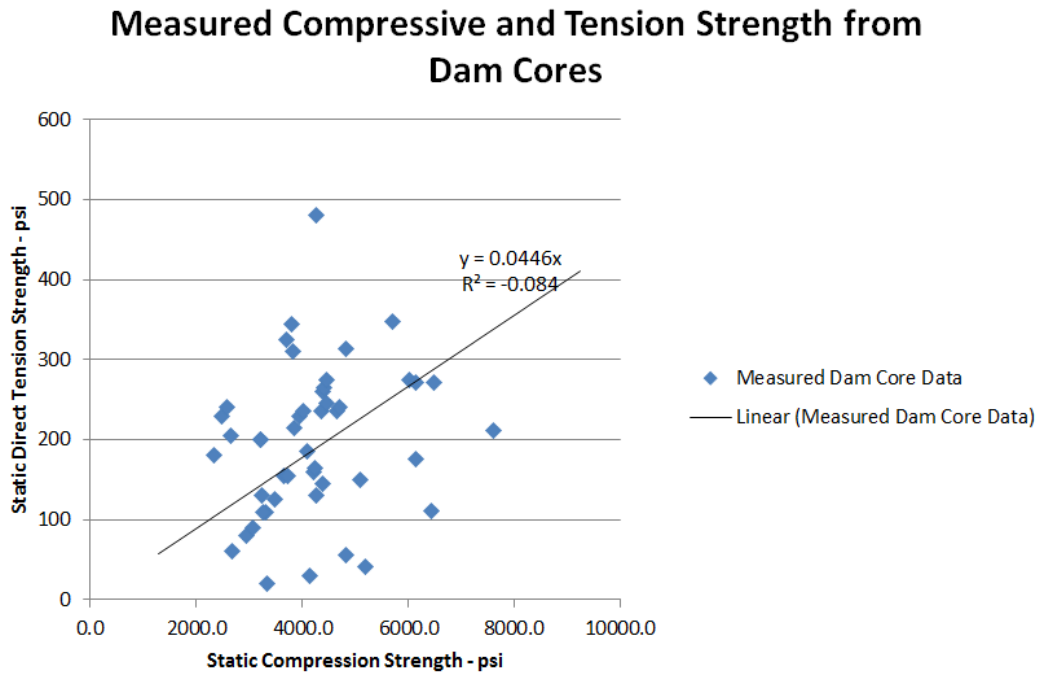
Figure 2.17.—Tensile and compressive strength data measured from dam cores.
(Data compiled by Harris; data courtesy of Materials Engineering and Research Laboratory)

Computerized structural analysis with three-dimensional meshes and nonlinear material models generally use a formulation that approximates a surface in stress space. Test data required to form such a surface are generally not available, particularly with dam materials. One dataset is shown on figure 2.18 for the
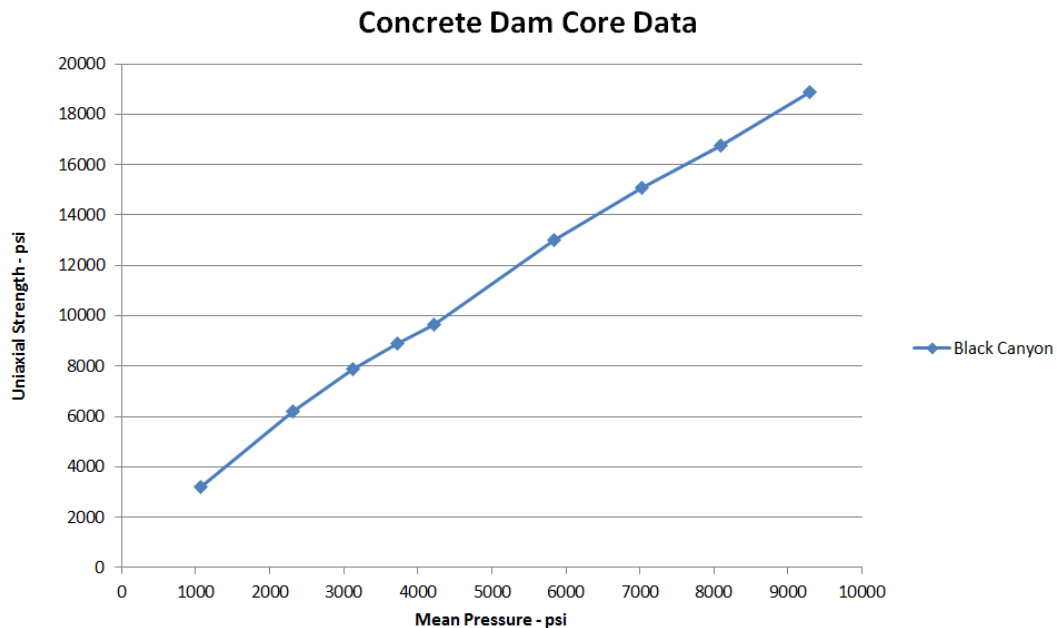
Figure 2.18.—Black Canyon Dam data with failure at varying confining pressures.
(Data compiled by Harris; data courtesy of Materials Engineering and Research Laboratory)

Black Canyon Dam materials (Madera, 2005). The data were produced using a triaxial cell with failures at different confining pressures. Thus, mean pressures versus deviator stresses at failure can be displayed.

The y-axis intercept of a surface may be expressed as the cohesion: $(\sigma_1 - \sigma_3)/2$, the deviator: $(\sigma_1 - \sigma_3)$, the second invariant: J_{2d}, or other forms depending on the model formulation. In any case, the intercept can be estimated using compressive and splitting tensile strength data in a Mohr-Coulomb format and converted to other forms as necessary. This construction is shown on figure 2.19 (left). The split cylinder data plots as a circle spanning the tension and compression sides of the x-axis owing to the biaxial tensile/compressive stress state of the test. The larger circle shown is a compression circle at 0 psi confining pressure. A shear surface is estimated by a line that is tangent to both circles, and the y-axis intercept found from this line intercept. The x-axis value at y = 0 should not be used for any value. Figure 2.19 (right) shows an alternate construction. In this figure, the data do not necessarily come from the same core run, but for both Mohr's circles, the minimum values were used. For these data, a linear fit is not the best fit, but rather, a bilinear fit produces a better fit to the data. This fit would be typical of plasticity models that use various curves to describe the failure surface.
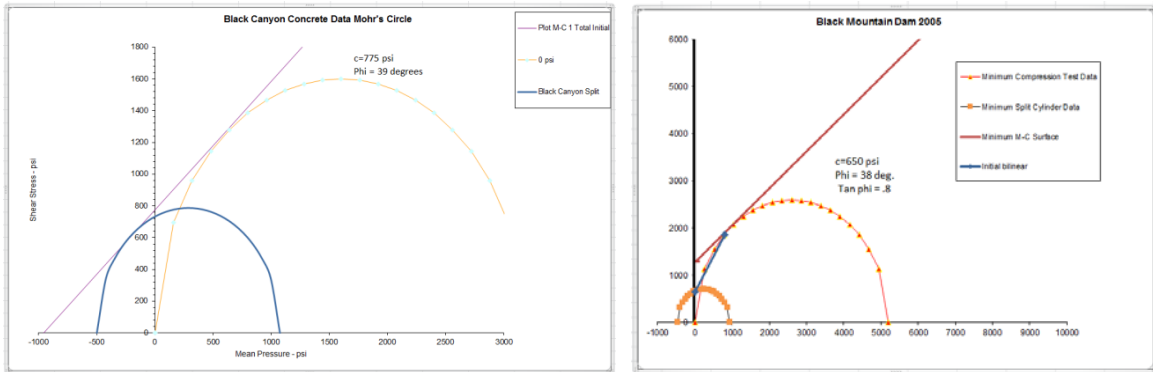
Figure 2.19.—Estimation of cohesion from splitting tensile and compressive strength data. Same core run with a linear fit (left) and two minimum cases with a bilinear fit (right). (Data compiled by Harris; data courtesy of Materials Engineering and Research Laboratory)

As mentioned previously, other types of data may be measured from dam cores. Presentations of multiple test methods are shown on figures 2.20 and 2.21. The figures show compression, tension, and shear test data. Data labeled as 30 years and 50 years are from cores sampled and tested in that age. All other data are taken from tests at early ages for the dam. Both static and dynamic test data are shown when available. Note in the Black Canyon data that the dynamic compressive strength is lower than the static compressive strength. For East Canyon Dam, dynamic strengths have a wider range with the maximum approximately equal to the static strength. This does not agree with what would be considered the intuitive pattern of dynamic values being greater than static values due to a strain rate effect. This effect is smaller in compression than in tension, and measured values do reflect this pattern. Measured values should be used when possible. In both cases, the dynamic splitting tensile strength is greater than the static strength. Also note the well-known trend that values reported from the split cylinder test are consistently higher than direct tension data; the values better approximate the direct shear cohesion values. Direct shear strength can be plotted as a zero pressure value when taken from the intercept of the normal stress/shear stress diagram.

Data from static and dynamic tests for Modulus of Elasticity and compressive strength are shown on figures 2.22 and 2.23, respectively. For dynamic tests, the strain rate was about 10^{-3}, which approximates dynamic movements of earthquakes. Careful study of the data reveals that not all cases show an increase in strength at higher strain rates as might be expected. Figure 2.24 shows data for cases of dynamic compression and static compression that could assist in estimating strengths when no higher strain rate data are available; a 10% increase in strength is indicated. Tensile strength increases were reported to be greater (Harris et al., 2000), with values reported for splitting tension tests as high as 1.4.
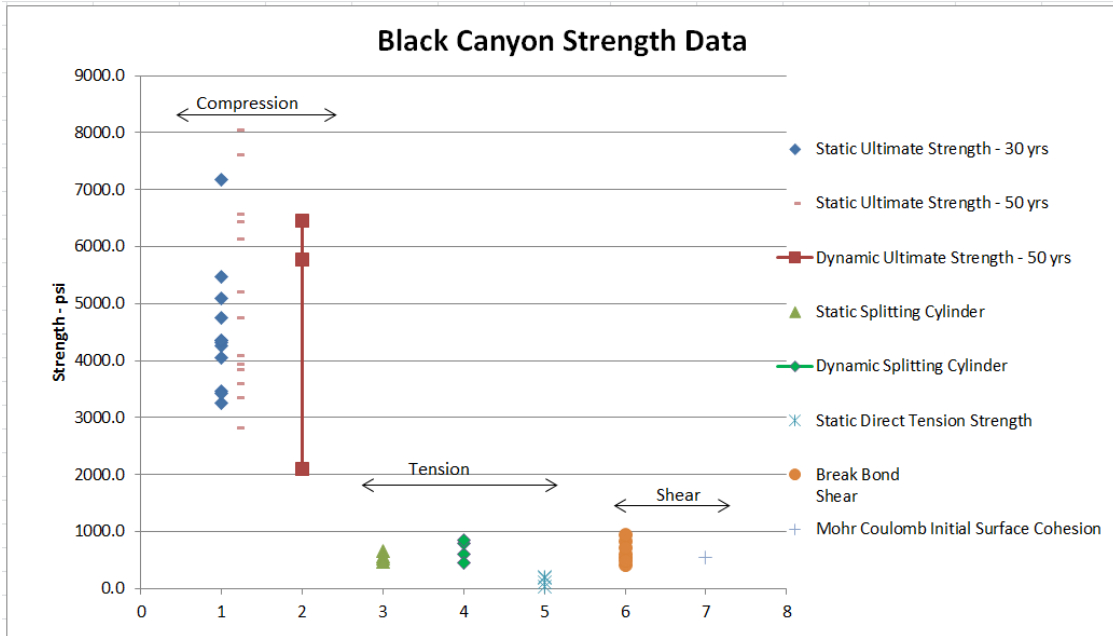
Figure 2.20.—Collection of various test data for Black Canyon Dam.
(Data compiled by Harris; data courtesy of Materials Engineering and Research Laboratory)
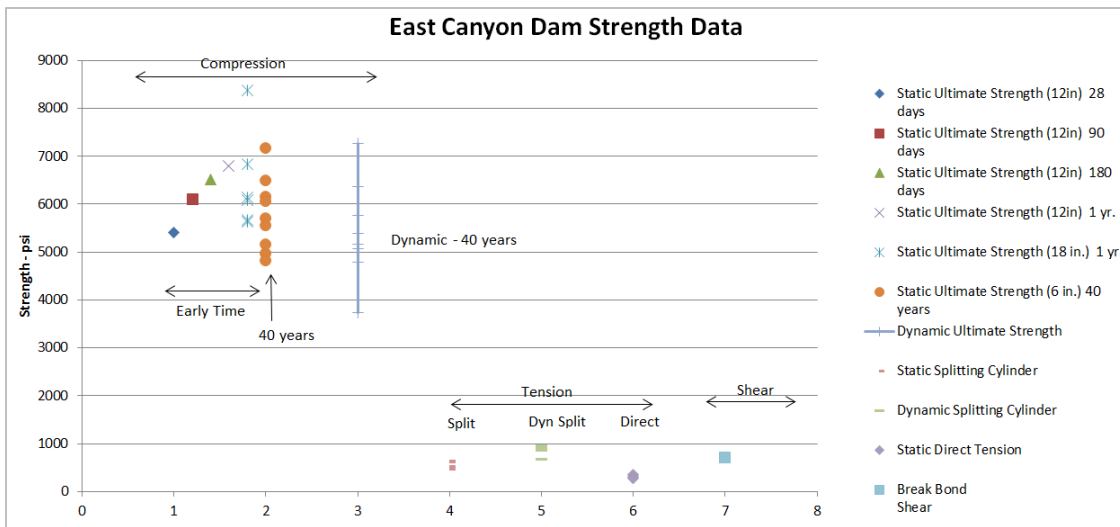
Figure 2.21.—Collection of various test data for East Canyon Dam.
(Data compiled by Harris; data courtesy of Materials Engineering and Research Laboratory)
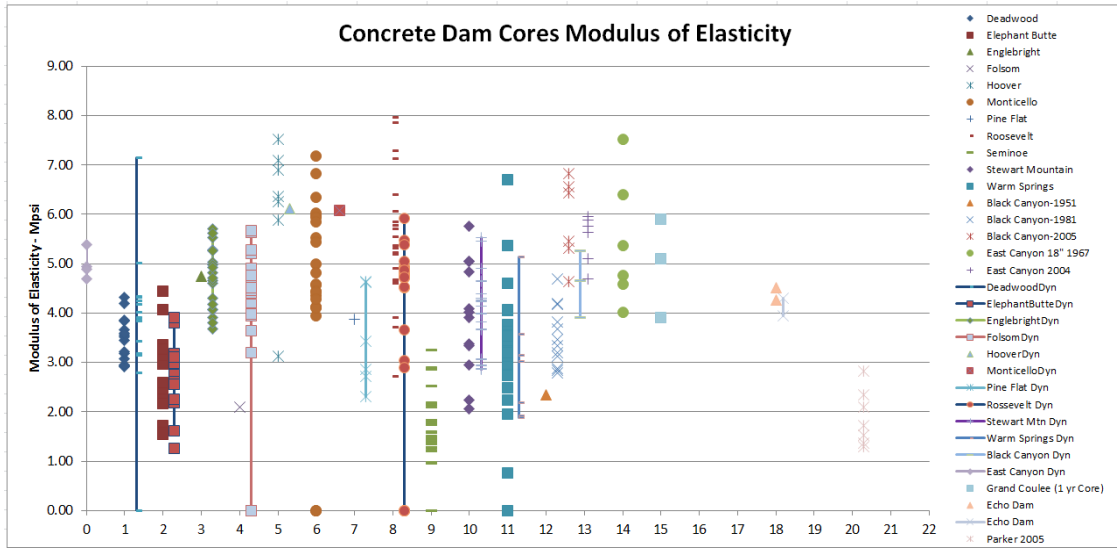
Figure 2.22.—Static (dots) and dynamic (connected dots) elastic modulus.
(Data compiled by Harris; data courtesy of Materials Engineering and Research Laboratory)
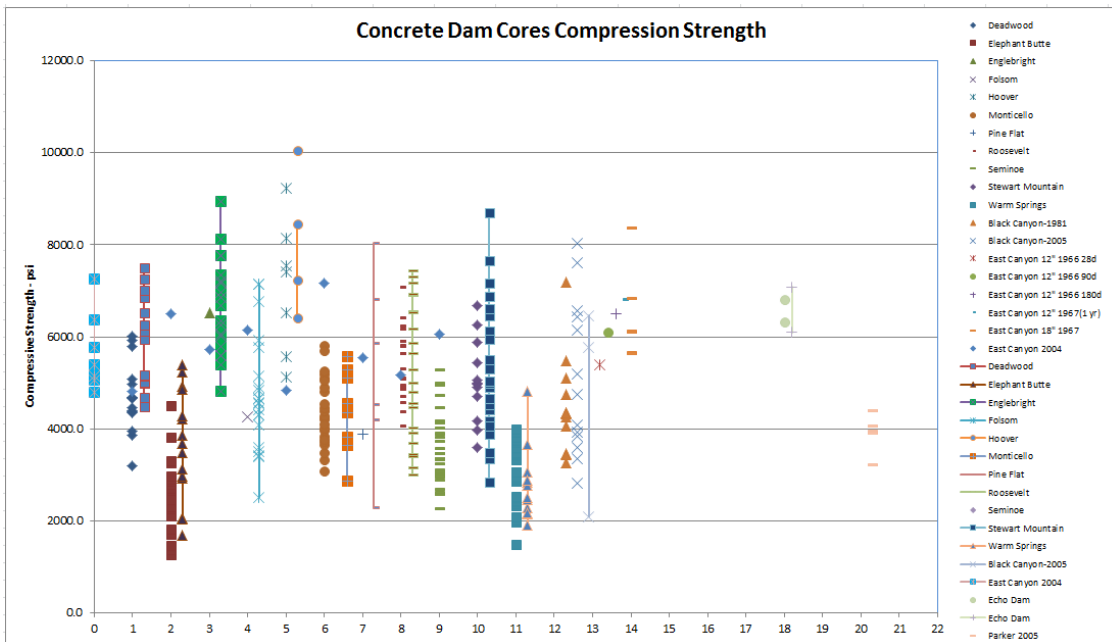
Figure 2.23.—Static (dots) and dynamic (connected dots) compressive strength.
(Data compiled by Harris; data courtesy of Materials Engineering and Research Laboratory)
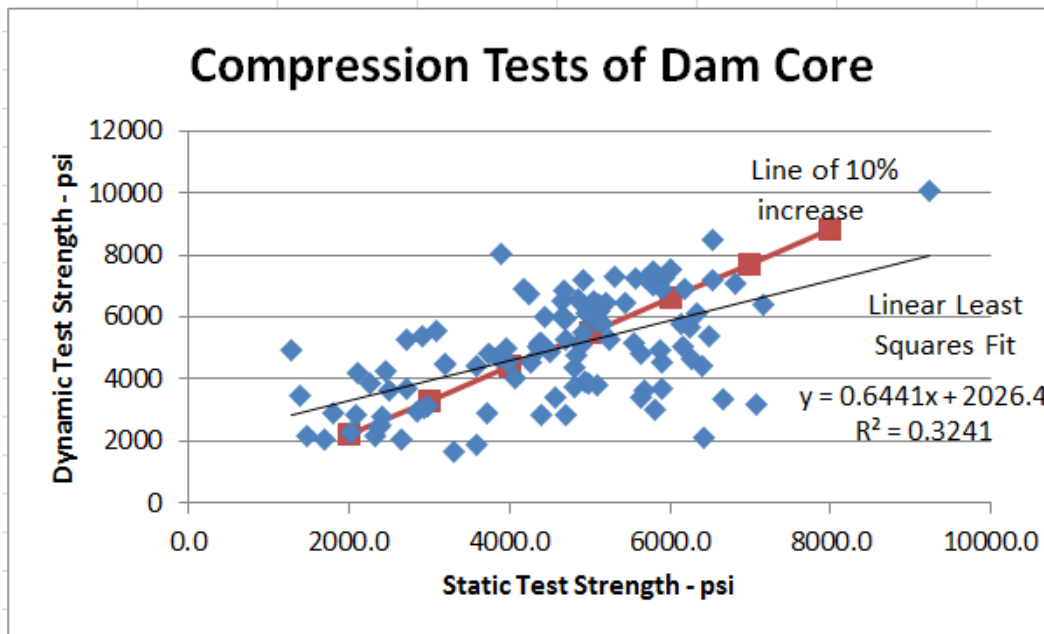
Figure 2.24.—Comparison of static to dynamic compressive strength.
(Data compiled by Harris; data courtesy of Materials Engineering and Research
Laboratory)

The discussion is this section (2.0) is based on comparisons of directly tested
values from cores retrieved from dams. Estimating input properties for nonlinear
computer material models is discussed in the following sections.

3.0　LABORATORY TESTING OF CONCRETE

In this section, standardized tests for measuring conventional concrete properties are presented. Many of the tests, particularly the ASTM tests, have a long history of use. These tests are used to find the linear elastic stiffness property of modulus and the ultimate compressive strength.

Other more modern tests are under ongoing development to directly measure the properties needed for nonlinear computer material models that utilize pressure versus strength surfaces and the onset of nonrecoverable strains.

Mechanical properties tests do not distinguish between mass and conventional concrete types, as the analysis and decisions are made on a stress/strain level. The same standard test procedures are used for both types.

3.1　Tests for Heat Properties of Conventional Concrete

As the interior temperature of mass concrete rises due to the process of cement hydration, the outer concrete may be cooling and contracting. If the temperature differs too much within the structure, the material can crack. The main factors influencing temperature variation in the mass concrete structure are the size of the structure, ambient temperature, initial temperature of the concrete at time of placement and curing program, cement type, and cement content of the mix.

Tests to measure heat properties of concrete are contained in USBR standards (Reclamation, 1992) and are summarized in the following section. These tests are used to design and evaluate mass concrete mixes, placement methods, and early age effects. Stresses due to thermal changes and temperature differentials can be analyzed with computer models using measured properties. These tests are abstracted briefly, as the emphasis of this report is the analysis of effects of loads on conventional concrete in dams, following the initial placement and paste gelling, or the majority of initial curing and hardening of the cement paste.

USBR 4907-92:　Procedure for Specific Heat of Aggregates, Concrete, and Other Materials

Specific heat is the amount of heat required to raise the temperature of a unit mass of material by 1 degree. The temperature regime and resulting thermal stresses in mass concrete, during its early life, are a function of the rate of heat evolution produced by cement hydration, specific heat, thermal conductivity, and density of

the concrete. Thus, knowledge of the thermal properties of concrete is necessary for establishing temperature control procedures during construction. A discussion by Dolen on this topic was contained in section 2.0

USBR 4909-92:   Procedure for Thermal Diffusivity of Concrete

Thermal diffusivity is an index of the facility of concrete to undergo temperature change. The coefficient of thermal conductivity can then be calculated, as it is the product of thermal diffusivity, specific heat, and saturated density of hardened concrete. Thermal conductivity is the rate at which heat is transmitted through a unit material, and the coefficient of thermal conductivity represents the uniform flow of heat through a thickness of material when subjected to a unit temperature difference between two faces.

USBR 4910-92:   Procedure for Coefficient of Linear Thermal Expansion of Concrete

The coefficient reports the strain due to a 1-degree temperature change. This coefficient is approximately constant for a considerable range of temperatures and generally increases with an increase in temperature.

USBR 4911-92:   Procedure for Temperature Rise of Concrete

When concrete is rapidly placed in a large mass structure, heat generated by the hydration of cement and pozzolan cannot be readily dissipated. Consequently, the structure reaches a high temperature while the concrete is still in a relatively plastic state. When cooling to normal temperatures does occur, concrete is less plastic, and thermally induced stresses may result in cracking of the structure if tensile strengths are exceeded. Special design and construction procedures are required to prevent cracking, which include artificial cooling of materials prior to mixing and/or embedded cooling pipes with the placement.

3.2   Tests for Mechanical Properties of Conventional Concrete

Tests used to define mechanical properties are summarized below. Linear, elastic properties of modulus and Poisson's ratio have been used extensively in structural analysis to calculate displacements and subsequently strains. These parameters can be directly measured in laboratory tests. In linear analyses, stresses are calculated from the modulus and strains and compared to values from laboratory tests or judgment to assess the safety of a structure.

National standards for tests provide the procedures and analysis of results for reporting standard parameters for concrete. Per ASTM, it is the responsibility of the user to determine the applicability of regulatory limitations prior to use. A characteristic of concrete placed in dams and, in general in structures made with large (greater than 3 feet) thicknesses, is the use of large aggregate to occupy volume and provide strength. The guidelines for specimen preparation or for coring of specimens are given in ASTM C-42.

**ASTM C42-13:   Standard Test Method for Obtaining and Testing Drilled
Cores and Sawed Beams of Concrete**

This standard highlights obtaining, preserving, and preparing samples for testing in compression, split cylinder testing, and beams tested in flexure. Considerations that affect the strength of concrete are presented as: location of the concrete in the structure – with concrete at the bottom generally stronger than at the top, cores obtained through the pour thickness generally stronger than cores obtained parallel to pour levels, and moisture content at the time of testing.

Earlier versions of this standard (2004 and 2010) noted that the preferred minimum core diameter is three times the nominal maximum size of maximum aggregate, but it should be at least two times the nominal maximum size of the coarse aggregate. However, the latest version (2013) merely states that the core diameter should be at least two times the nominal maximum size of the coarse aggregate. Six-inch-diameter cores are commonly used, but most concrete in Reclamation dams generally contains aggregates larger than 2 inches as noted in section 2.1.

This requirement virtually eliminates direct comparison of concrete cored from dams and suites of laboratory prepared tests. Concrete dam cores need to be drilled through material that contains 6-inch aggregate and larger, while laboratory prepared specimens are made under ideal laboratory conditions with aggregate proportioning and curing conditions. Tests made solely from laboratory specimens will generally yield higher strength values, and careful judgment needs to be made to compare to actual conditions of field structures.

The following tests find scalar values as properties of concrete. As noted previously, modulus is used to formulate the analysis, while strength values are used as a comparison to calculated values to judge strength.

**ASTM C39-14:   Standard Test Method for Compressive Strength of
Cylindrical Concrete Specimens (USBR 4039)**

This well-known test uses a uniaxial linearly increasing compression load to fail an unconfined cylinder. The highest recorded load is divided by the initial area and reported as compressive strength.

ASTM C78 -10:   Standard Test Method for Flexural Strength of Concrete (Using Simple Beam with Third Point Loading)

This test is not commonly used with dam materials; it is common in pavements. The flexural strength is readily found from the bending equation.

ASTM C469-14   Standard Test Method for Static Modulus of Elasticity and Poisson's Ratio of Concrete in Compression (USBR 4469)

This test uses the same procedure as C39-14, but adds a compressometer for the measurement of displacements used to find strain. Longitudinal strain is used with stress to find the Modulus of Elasticity as a chord modulus from the pair of points at a strain of 0.000050 inch per inch (50 microstrain) and a stress of 0.40 of the maximum. USBR 4469 recognizes strain gages for the measurement of longitudinal and lateral strains directly. Lateral strain is used as a ratio with longitudinal strain to find Poisson's ratio. Reclamation's laboratory test setup is shown on figure 3.1. Strain and calculated modulus data shown in section 2 are from the Reclamation laboratory tests measured using this setup.
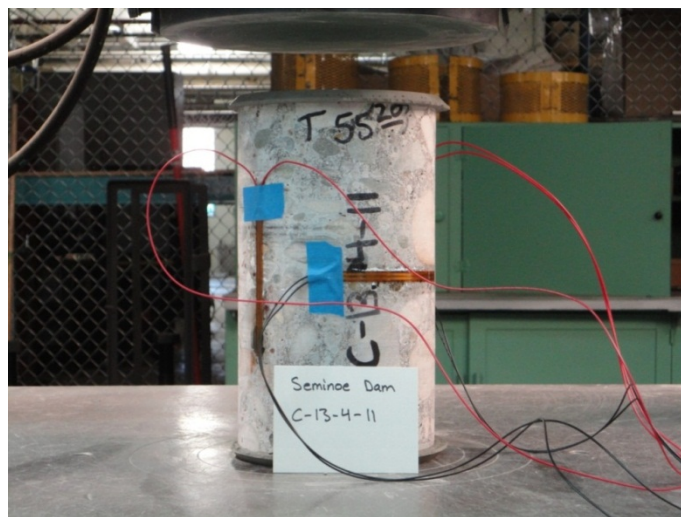
Figure 3.1.—USBR 4469 test setup.
(Photo: Reclamation – Materials Engineering and Research Laboratory)

ASTM C496-11   Standard Test Method for Splitting Tensile Strength of Cylindrical Concrete Specimens

This test places a bar along the length of a cylinder and applies a compression load to split the cylinder. Equations from the Theory of Elasticity are used to suggest a tensile stress, but care must be used to compare the values to the correct biaxial stress state. Recent work by Dolen (Dolen et al., 2014) also discusses size effects and other parameters affecting the calculated values.

**USBR 4914 Direct Procedure for Direct Tensile Strength, Static Modulus
of Elasticity, and Poisson's Ratio of Cylindrical Concrete
Specimens in Tension**

This test uses glued end plates on cylinders and a tension load to find the failure
stress, the direct tensile strength.

USBR 4915 Procedure for Direct Shear of Cylindrical Concrete Specimens

This test uses a normal load and a lateral, shearing load to fail a sample. Multiple
normal loads are used to form a relationship between normal stress and shear
stress that can be analyzed as a Mohr-Coulomb, or other, surface. A failed, or
existing plane such as a lift line, can be tested to give a residual strength.

3.3 Tests Adopted for Concrete Testing to Extend Data to Surfaces

Relationships have been theorized for nonlinear material behavior relating to
stress and pressure effects for plastic and brittle failure predictions. These various
relationships have been used to formulate different nonlinear material models in
computer programs. Some laboratory tests have been developed to derive
parameters for various nonlinear models. These tests are not currently codified as
standard tests. Many models assume characteristic shapes for the relationship of
stresses as a function of three-dimensional mean pressures and use the uniaxial
strength to adjust maximum possible values. Data from some of the laboratory
tests can be combined to assist in the development of stress/pressure relations.

Dynamic Compressive and Splitting Tensile Strength

ASTM C469 and ASTM C496 can be run using faster machine speeds to produce
the same parameters, but the parameters can be compared to the slower test to
evaluate the effect of strain rate.

**ASTM D2850-03: Standard Test Method for Unconsolidated-Undrained
Triaxial Compression Test on Cohesive Soils**

This test is conducted with a confining pressure and a longitudinal load used to
fail a cylinder. Unlike previously described tests, this test is used with a series
of samples to produce a shear strength surface. Such a surface is used with
nonlinear material models.

Valuable data from the first stage of testing is the data record from the application
of a uniform, hydrostatic load while recording volumetric strain. The data
are typically plotted as pressure versus volumetric strain, the slope of which,

assuming elastic theory, is the bulk modulus, K. The data can be used to find compression characteristics common to many models. The data are used to find cap parameters described in Model 159 and Equation of State (EOS) parameters described in Model 72R3.

The second phase of the test, the shear phase, holds the desired confining pressure constant, and the axial load is increased until the specimen fails. The shear data are generally plotted as principal stress difference versus axial strain, the slope of which is Young's modulus, E. By using varying confining pressures and longitudinal loads, the shear strength as a function of confining pressure is found. Data are commonly displayed as a failure surface, such as a Mohr-Coulomb surface, or as mean pressure versus deviator stress (shear stress).

Uniaxial Tests with Unload/Reload Cycles

The ASTM C469 test can be modified to use unload and reload cycles at increasing strain levels. The data are plotted as a stress-strain graph. The data can be analyzed to show changes in Young's modulus as a function of stress level by calculating the slope of each unload/reload cycle. In addition, the accumulation of plastic strain is demonstrated at the end of each unload cycle. The latter data can be used to aid in finding parameters related to damage of concrete.

For dynamic analyses, material damping can also be calculated from the data.

Triaxial Extension Tests

The triaxial extension test is run in the same chamber as the triaxial compression (TXC) test. For the extension test, the confining pressure is increased, and the cylinder expands longitudinally, or the confining pressure is held constant, and the axial stress reduced. The data produce extension data of the cylinder.

Uniaxial Strain Tests

A uniaxial strain test is conducted by simultaneously applying axial load and confining pressure so that as the cylindrical specimen is shortened, its diameter remains unchanged (i.e., zero radial strain boundary conditions are maintained). The data are generally plotted as axial stress versus axial strain, the slope of which is the constrained modulus, M. The data are also plotted as principal stress difference versus mean normal stress, the slope of which is twice the shear modulus, G, divided by the bulk modulus, K (i.e., 2G/K) or in terms of Poisson's ratio, ν, $3(1-2\nu)/(1+\nu)$.

4.0 DESCRIPTION OF CONCRETE MATERIAL MODELS

The safety of the design of concrete dams is well-established in the engineering practice using linear-elastic models of concrete. However, investigation results have shown that linear models do not adequately represent the performance of concrete dams during earthquakes. Since microcracks are expected to form and propagate during large earthquakes, the performance of mass concrete in dam structures is nonlinear, and it is a very complex phenomena. There have been many attempts to model behavior and fracture of concrete dams. Three major approaches can be identified with mechanics of materials:

- *Discrete crack model*, based on principals of fracture mechanics, assumes a crack as a geometrical discontinuity. The discrete crack approach provides good results for monotonic loads and stationary cracks, but it gives relatively poor accuracy for crack propagation problems and cyclic loads. The approach may be inefficient in the analysis of concrete dams under seismic load conditions.

- *Smeared crack model*, based on principals of continuum mechanics, describes damage to the material in terms of changing material properties. Though the smeared crack model is convenient in a numerical analysis, it has many limitations in respect to crack direction, cyclic-loading and unloading, and combining cracking with other inelastic phenomena.

- *Plastic-damage based models*, based on principals of continuum mechanics, represent fracture of the material by equivalent continuum strains. Damage of the material is assumed to be limited by the state of plastic yielding. Several versions of material damage models have been developed, including plasticity softening models, elasto-damage models, elasto-plastic damage models, or gradient plasticity models. The most important feature of the plastic-damage models are the damage properties that are observed in quasi-brittle materials like concrete and the ability to model the plastic hardening and softening as well as tensile failure in the constitutive equation.

Among these three general approaches, the plastic-damage models appear to be the most appropriate for modeling mass concrete dam behavior exhibited under cyclic earthquake loads.

The theory of the plastic-damage models, represented by the KCC model and the CSCM, is presented in this section. The CSCM is relatively new and is introduced here for the first time for the analysis of concrete dams. The KCC model is also presented. Both models provide the capability to input a compressive strength value and have all other needed parameters estimated from

previous test suites. For the CSCM estimation procedures, data from CEB (CEB 1993) for conventional concrete tests are used. The KCC model estimation procedures are based on Joy and Moxley (1993) data, which are also used in the CSCM for strain rate effects.

Both the CSCM and the KCC model employ three shear strength surfaces: the yield surface, the limit surface, and the failure surface. The two models differ in their softening evolution equations and in the equations describing degradation of the elastic stiffness (the strain-to-failure is tied to fracture energy release). The KCC model uses an accumulating damage model that adjusts the current strength within any given time step to a stress state varying between the three strength curves used in the model, whereas the CSCM uses Duvaut-Lion visco-plasticity theory to give a smoother prediction of transient effects. Both models support rate dependence by allowing the strength curves to be a function of strain rate.

4.1   Continuous Surface Cap Model

The CSCM was developed for roadside safety analysis in the 1990s by APTEK, Inc., and was made available in LS-DYNA in 2005. The CSCM is an elasto-plastic damage material model with rate effects and is equipped with two surfaces: the failure surface and hardening cap. A continuous intersection is maintained between the surfaces. The main features of the model are:

- Three stress invariant yield surface
- A hardening cap that expands and contracts
- Plasticity-damage-based softening with erosion and modulus reduction
- Rate effect for increasing strength in high-strain rate applications
- Automated parameter generation scheme based on the uniaxial compressive strength, f'_c

Major advantages of this model are the ability to control the amount of dilatancy produced under shear loading and the ability to model plastic compaction. The model is based on the general theory published by Simo and Ju (1987a and 1987b) and implemented with some modifications in LS-DYNA by Murray (2007).

4.1.1   Description of the Model

The yield surface of the CSCM material is defined by two surfaces: the *shear failure surface* and a *hardening cap* with a smooth intersection between these surfaces. The general shape of the yield surface and its section in the meridional plane is shown on figure 4.1.
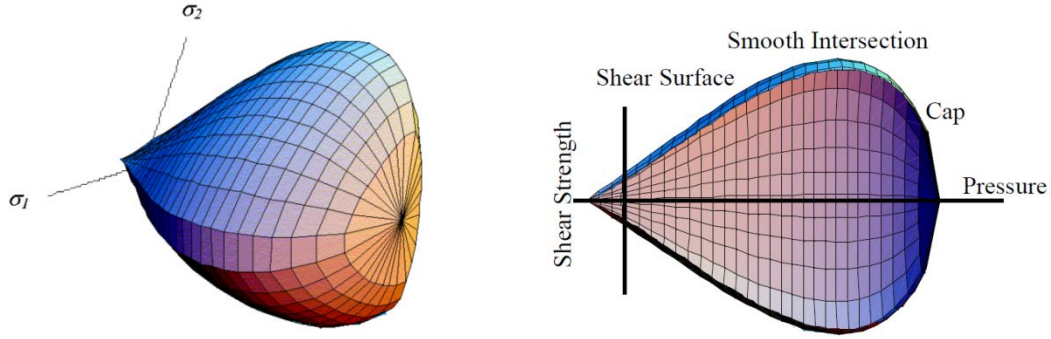
Figure 4.1.—General shape of CSCM yield surface in three dimensions and its section in meridional plane, Murray (2007).

The smooth intersection eliminates the numerical complexity of treating a transition region between the failure surface and cap. This type of model is often referred to as *a smooth cap model* or as a *continuous surface cap model*. The yield function for the CSCM is based on three stress tensor invariants and the cap hardening parameter, κ, as follows:

$$f(J_1, J_2', J_3', \kappa) = J_2' - \Re^2 F_f^2 F_c$$

(Eq. 1)

Here F_f is the shear failure surface, F_c is the hardening cap, and $\Re$ is the Rubin three-invariant reduction factor. Multiplying the cap ellipse function by the shear surface function allows the cap and shear surfaces to take on the same slope at their intersection. The yield surface could be formulated in terms of three stress invariants of the stress tensor because an isotropic material has three independent stress invariants.

4.1.2   Shear Failure Surface

The strength of a material is modeled by the shear surface in the tensile and low confining pressure regimes. The shear surface F_f is defined along the compression meridian by the equation:

$$F_f(J_1) = \alpha - \gamma e^{-\beta J_1} + \theta J_1$$

(Eq. 2)

Values of α, β, γ, θ parameters are selected by fitting the model surface to strength measurements from TXC tests conducted on cylinders (and then adjusting these parameters to account for compaction and damage). The TXC

data are typically plotted as principal stress difference versus pressure. The principal stress difference (axial stress minus confining stress) is equal to the square root of $3J'_2$. The shear surface is shown on figure 4.2.
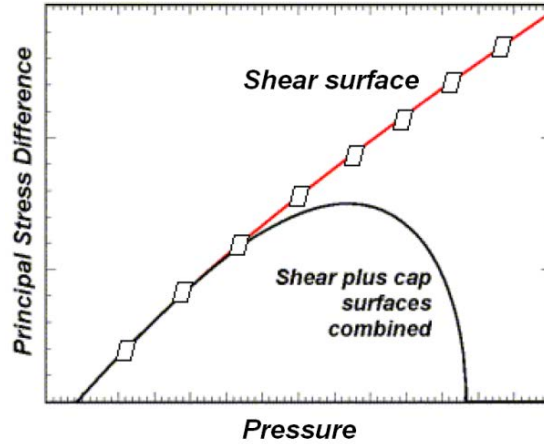
Figure 4.2.—General shape of CSCM yield surface in two dimensions.

4.1.3   Cap Model Compaction Surface

The cap is used to model plastic volume change related to pore collapse (although the pores are not explicitly modeled). The initial location of the cap determines the onset of the plasticity zone in isotropic compression and uniaxial strain. The elliptical shape of the cap allows the onset for isotropic compression to be greater than the onset for uniaxial strain, in agreement with shear enhanced compaction data. The motion of the cap determines the shape (hardening) of the pressure-volumetric strain curves via fits with data (without cap motion, the pressure-volumetric strain curves would be perfectly plastic).

The isotropic hardening cap is a two-part function that is either unity or an ellipse. When the stress state is in the tensile or very low confining pressure region, the cap function is unity: yield strength via the equation is independent of the cap. When the stress state is in the low to high confining pressure regimes, the cap function is an ellipse: yield strength depends on both the cap and shear surface formulations. The two-part cap function is defined by equation 3.

$$F_c(J_1, \kappa) = 1 - \frac{[J_1 - L(\kappa)] \left[|J_1 - L(\kappa)| + J_1 - L(\kappa) \right]}{2 \left[X(\kappa) - L(\kappa) \right]^2}$$

(Eq. 3)

where $X(\kappa)$ is the intersection of the cap surface with the J_1 axis, and $L(\kappa)$ is defined by

$$L(\kappa) = \begin{cases} \kappa & if \ \kappa > \kappa_o \\ 0 & otherwise \end{cases}$$
(Eq. 4)

The cap moves to simulate plastic volume change. The cap expands ($X(\kappa)$) and κ increases) to simulate plastic volume compaction. The cap contracts ($X(\kappa)$ and κ decreases) to simulate plastic volume expansion (called dilation). The expansion and contraction of the cap is based on the hardening rule, expressed by equation 5.

$$\varepsilon_v^p = W\left[1 - e^{-D_1(X-X_0)-D_2(X-X_0)^2}\right]$$
(Eq. 5)

The five input parameters (X_0, W, D_1, D_2, and the cap aspect ratio R) are obtained from fits to the pressure-volumetric strain curves in isotropic compression and uniaxial strain and are graphically explained on figure 4.3. The cap initial location, X_0, determines the pressure at which compaction initiates in isotropic compression; R combined with X_0 determines the pressure at which compaction initiates in uniaxial strain; D_1 and D_2 determine the shape of the pressure volumetric strain curves; and W determines the maximum plastic volume compaction.
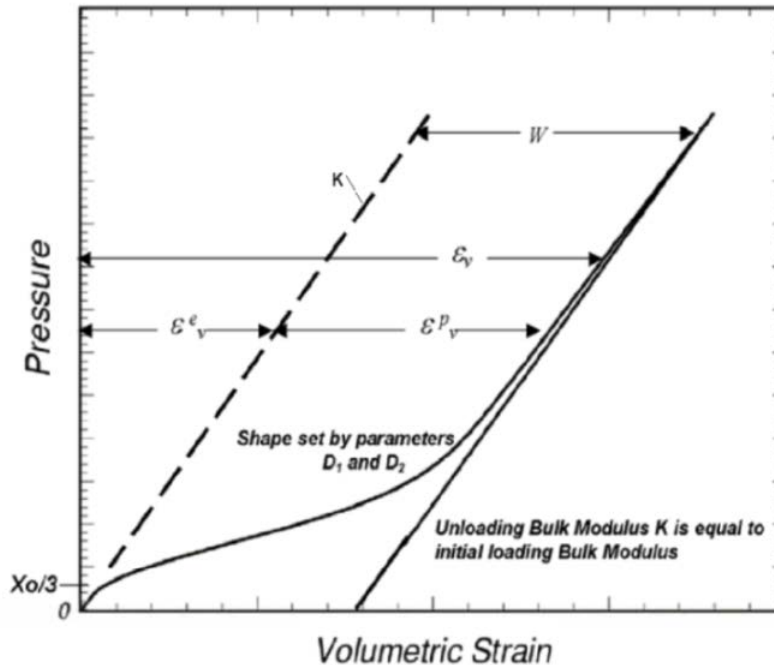
Figure 4.3.—Pressure-volumetric strain curve for CSCM.

4.1.4   Rubin Scaling Function

If the material fails at lower values of J'_2 for TXE and TOR tests than it does for TXC tests that are conducted at the same pressure, then the material strength depends on the third invariant of the deviatoric stress tensor, J'_3. When viewed in the deviatoric plane, a three-invariant yield surface is triangular or hexagonal in shape as shown on figure 4.4. The Rubin scaling function, $\Re$, determines the material strength for any state of stress relative to the strength for TXC. Strengths like TXE and TOR are simulated by scaling back the TXC shear strength by the Rubin function: $\Re F_f$. The Rubin function is a scaling function that changes the shape (radius) of the yield surface in the deviatoric plane as a function of angle as shown on figure 4.4. This shape may be a circle (Drucker-Prager or von Mises Models), a hexagon (Mohr-Coulomb Model), or an irregular hexagon-like shape (Willam-Warnke Model) in which each of six sides is quadratic between the TXC and TXE states.
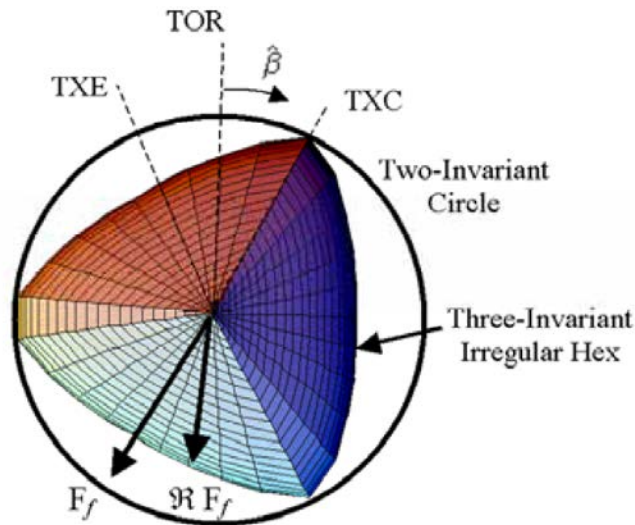
Figure 4.4.—Illustration of two- and three-invariant shapes of the concrete material model in the deviatory plane, Murray (2007).

For comparison, a two-invariant model cannot simultaneously model different strengths in TXC, TXE, and TOR. When viewed in the deviatoric plane, the two-invariant yield surface is a circle as shown on figure 4.4. A two-invariant formulation is modeled with the Rubin function equal to $\Re = 1$ at all angles around the circle. This means that the TXC, TOR, and TXE strengths are modeled the same.

4.1.5   Kinematic Hardening

In compression at low confined pressure, the stress-strain behavior of concrete typically exhibits nonlinearity and dilation prior to the peak. This type of behavior is modeled in CSCM with an initial shear yield surface, $N_H F_f$, which hardens until it coincides with the ultimate shear yield surface, F_f. Two input parameters are required: N_H that initiates hardening by setting the location of the initial yield surface as a fraction of the final yield surface and C_H that determines the rate of hardening (amount of nonlinearity).

4.1.6   CSCM Implemented in LS-DYNA

The CSCM is implemented in LS-DYNA as material model No. 159. The user can use an option "concrete" (*MAT_CSCM_CONCRETE), and the model will generate default material properties. The "concrete option" uses a set of standardized material properties generated for three basic user's input parameters: the unconfined compressive strength, the aggregate size, and the units. The parameters are fit to data for unconfined compressive strengths between about 20 and 58 MPa (2,901 to 8,412 psi), with emphasis on the midrange between 28 and 48 MPa (4,061 and 6,962 psi). The unconfined compressive strength affects all aspects of the fit, including stiffness, three- dimensional yield strength, hardening, and damage. The fracture energy affects only the softening behavior of the damage formulation. Softening is fit to data for aggregate sizes between 8 and 32 millimeters (0.3 and 1.3 inches) (Murray, 2007). The suite of material properties for Model 159 was primarily obtained through use of the CEB-FIP Model Code (CEB, 1993).

The user has also an option of inputting his own material properties by selecting the "blank" option (*MAT_CSCM).

4.1.7   Modulus Values G and K

Modulus values in the CSCM are automatically generated based on a relationship of uniaxial compressive strength. The base equation is from the CEB (1993):

$$E = E_{CEB} \, (f'_c/10)^{1/3} \qquad\qquad \text{(Eq. 6)}$$

where E is Young's modulus, and the default value of $E_{CEB} = 18.275$ MPa (2,651 psi), which is the value of Young's modulus when $f'_c = 10$ MPa (1,450 psi). This value of E_C is for simulations that are modeled linear to the peak (no pre-peak hardening). The isotropic moduli are found using the isotropic equations:

$$G = \frac{E}{2(1+v)} \qquad \text{and} \qquad K = \frac{E}{3(1-2v)},$$

$$\text{(Eq. 7)}$$

These values from table 4.1 are compared to data from tested dam cores on figure 2.15. It can be seen that the estimating equation produces values that pass through actual measured values but are too low at higher values of compressive strength.

Note: It is recommended that for analyses of Reclamation concrete dam's values of Young's modulus that actual cores and laboratory data be used. If no tested values are available, then it is suggested that values be taken from a family of sites that are similar to the analysis case. Mass concrete Poisson's ratio values measured in the lab are generally between 0.19 and 0.25, with 0.21 a typical value. Once these two values are established, a shear modulus and bulk modulus value can be determined using the isotropic equations.

Table 4.1.—Default bulk and shear moduli of concrete derived from equations 6 and 7 per CEB

Unconfined Compression Strength MPa (psi)	Young's Modulus GPa (ksi)	Poisson's Ratio	Bulk Modulus GPa (ksi)	Shear Modulus GPa (ksi)
20 (2,901)	23.0 (3,336)	0.15	11.0 (1,595)	10.0 (1,450)
28 (4,061)	25.8 (3,742)	0.15	12.3 (1,784)	11.2 (1,624)
38 (5,511)	28.5 (4,134)	0.15	13.6 (1,973)	12.4 (1,798)
48 (6,962)	30.8 (4,467)	0.15	14.7 (2,132)	13.4 (1,944)
58 (8,412)	32.8 (4,757)	0.15	15.6 (2,263)	14.3 (2,074)

4.1.8 Triaxial Compression Surface

The TXC yield surface, equation 8, relates strength to pressure via four parameters: α, λ, β, and Θ.

$$TXC\ Strength = \alpha - \lambda e^{-\beta J_1} + \theta J_1 \qquad \text{(Eq. 8)}$$

CEB's uniaxial compression and tension measurements from table 4.2 are used in table 4.3 to set default TXC yield surface parameters.

Table 4.2.—CEB's strength measurement used to set default TXC yield surface
parameters

Measurement Type	Strengths Set 1	Strengths Set 2	Strengths Set 3	Strengths Set 4	Strengths Set 5
Uniaxial Compression f'_c MPa (psi)	20 (2,901)	28 (4,061)	38 (5,511)	48 (6,962)	58 (8,412)
Uniaxial Tension f'_T MPa (psi)	1.6 (232)	2.2 (319.1)	2.9 (421)	3.5 (508)	4.1 (595)
Triaxial Tension MPa (psi)	1.6 (232)	2.2 (319.1)	2.9 (421)	3.5 (508)	4.1 (595)
Triaxial Compression $2.75 f'_c$ at P = $1.5 f'_c$ MPa (psi)	55 (7,977)	77 (11,168)	105 (15,229)	132 (19,145)	160 (23,206)

Table 4.3.—TXC yield surface parameters as a function of unconfined compressive
strength

Unconfined Compression Strength MPa (psi)	α MPa (psi)	λ MPa (psi)	β MPa^{-1} (psi^{-1})	θ
20 (2,901)	12.8 (1,856)	10.5 (1,523)	1.929E-02	0.266
28 (4,061)	14.2 (2,060)	10.5 (1,523)	1.929E-02	0.290
38 (5,511)	15.4 (2,234)	10.5 (1,523)	1.929E-02	0.323
46 (6,672)	15.9 (2,306)	10.5 (1,523)	1.929E-02	0.350
58 (8,412)	15.9 (2,306)	10.5 (1,523)	1.929E-02	0.395

The CSCM calibration parameters from table 4.3 are illustrated on figure 4.5
along with data from Black Canyon Dam conventional triaxial tests (discussed
earlier in section 2.0).

It can be seen on figure 4.6 that the Black Canyon data with measured unconfined
compressive strength of 3,200 psi show values above all CEB (CSCM default)
data. The approximation used in the material model for the TXC shear failure
surface was described above with equation 2. This surface equation is readily fit
and compares favorably to the conventional triaxial data as shown on figure 4.6
with values for α, λ, β, and Θ set to 1,300, 1,523, 1.93E-02, and 0.8, respectively
(rather than using a value of f'_c and autogeneration. Note from figure 2.19 (right)
that the alpha value is taken as two times the cohesion, which is typical as
$c = (\sigma_1 - \sigma_3)/2$ and the intercept does not use the division by 2 (so alpha =
1,300 rather than c = 650 psi.), and that the theta value is taken as tan ϕ from the
Mohr-Coulomb fit. The variables λ and β are held constant typical to values in
table 4.3.
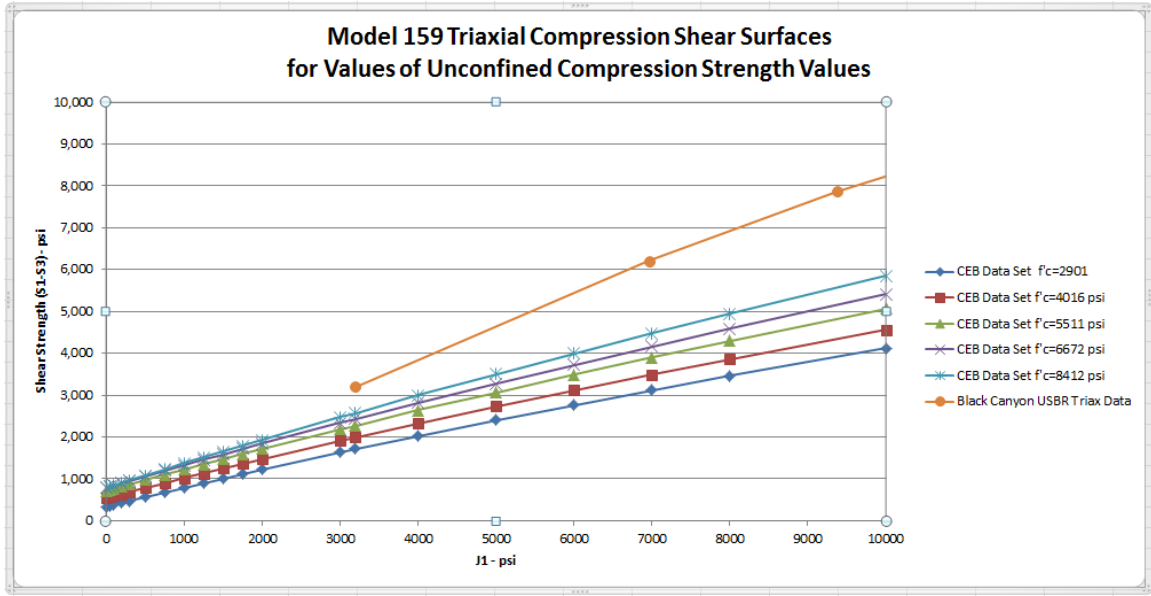
Figure 4.5.—Default CSCM parameters for TXC compared with Black Canyon Dam concrete test data.
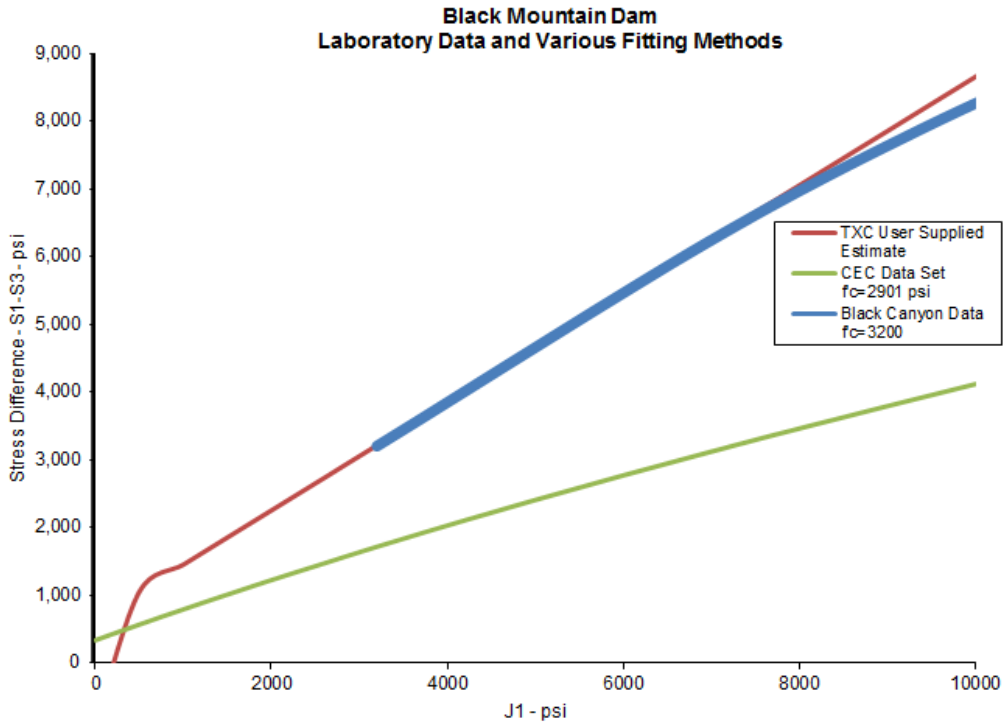
Figure 4.6.—Fit CSCM material TXC shear surface to Black Canyon Dam concrete test data.

Unfortunately, triaxial test data for dam cores is scarce. An alternative would be to form a shear failure surface using a Mohr-Coulomb graph with unconfined compression data and split cylinder data as discussed previously, shown on figure 2.19, and as shown above.

4.1.9   Triaxial Extension and Torsion Surface

Triaxial torsion and triaxial extension surface, defined by equations 9 and 10, respectively, could be expressed by the Rubin scaling function relative to the TXC strength. The Rubin function may remain constant or vary with pressure.

$$Q_1 = \alpha_1 - \lambda_1 e^{-\beta_1 J_1} + \theta_1 J_1 \qquad \text{(Eq. 9)}$$

$$Q_2 = \alpha_2 - \lambda_2 e^{-\beta_2 J_2} + \theta_2 J_2 \qquad \text{(Eq. 10)}$$

4.1.10   Cap and Hardening Parameters

The cap parameters in the CSCM are determined by fitting pressure-volumetric strain curves based on hydrostatic compression or uniaxial strain tests. Cap and hardening parameters as a function of unconfined compression strength for default fits are listed in table 4.4 and presented on figure 4.3.

Table 4.4.—Cap and hardening parameters as a function of unconfined compressive strength

Unconfined Compression Strength MPa (psi)	Cap Shape R	Cap Location Xo MPa (psi)	Maximum Plastic Volume Change W	Linear Hardening D_1 MPa (psi)	Quadratic Hardening D_2 MPa^2 (psi^2)
20 (2,901)	5	87 (12,618)	0.05	2.50e-04	3.49e-07
28 (4,061)	5	90 (13,053)	0.05	2.50e-04	3.49e-07
38 (5,511)	5	95 (13,779)	0.05	2.50e-04	3.49e-07
48 (6,962)	5	102 (14,794)	0.05	2.50e-04	3.49e-07
58 (8,412)	5	110 (15,954)	0.05	2.50e-04	3.49e-07

4.1.11   Evolution of Damage

Concrete softens in the tensile and low confining pressure conditions. Fracture energy is given by CEB equation 11:

$$G_F = G_{F0} \left(\frac{f_c'}{10} \right)^{0.7} \qquad \text{(Eq. 11)}$$

where the fracture energy coefficient of G_{F0} is given from CEB tests as shown in table 4.5.

Table 4.5.—Fracture energy coefficients as a function of compressive strength and aggregate size

Unconfined Compression Strength MPa (psi)	8-mm (0.31-inch) Aggregate KPa-cm (psi-inches)	16-mm (0.62-inch) Aggregate KPa-cm (psi-inches)	32-mm (1.26-inch) Aggregate KPa-cm (psi-inches)
20 (2,901)	4.0	5.0	6.5
28 (4,061)	5.0	6.0	8.0
38 (5,511)	6.5	7.5	9.5
48 (6,962)	7.0	9.0	1.15
58 (8,412)	8.5	1.05	1.30

1 KPa-cm = 0.05710 Psi-inch

4.1.12   Strain Rate

Concrete exhibits an increase in strength and elastic modulus with increasing strain rate (refer to section 4.2.3). The dynamic increase factor (DIF) in the CSCM (a ratio between the dynamic and static strength) shown on figure 4.7 is based on the developer's experience on various defense projects, particularly for concrete with a strength of 6,500 psi (Joy and Moxley, 1993).

4.2   Karagozian Case Concrete Material Model

4.2.1   Introduction

The work undertaken by K&C on the development of a material model for reinforced concrete resulted in the first release of the KCC Model in 1994. The second release implemented in LS-DYNA in 1996 was followed by the third release in 1999 that is used in the current version of LS-DYNA. However, K&C is working on the release of a new KCC model R4 that will be implemented in LS-DYNA. The KCC model was specifically created to improve the analysis of reinforced concrete to high-velocity pressure wave effects. It exhibits several
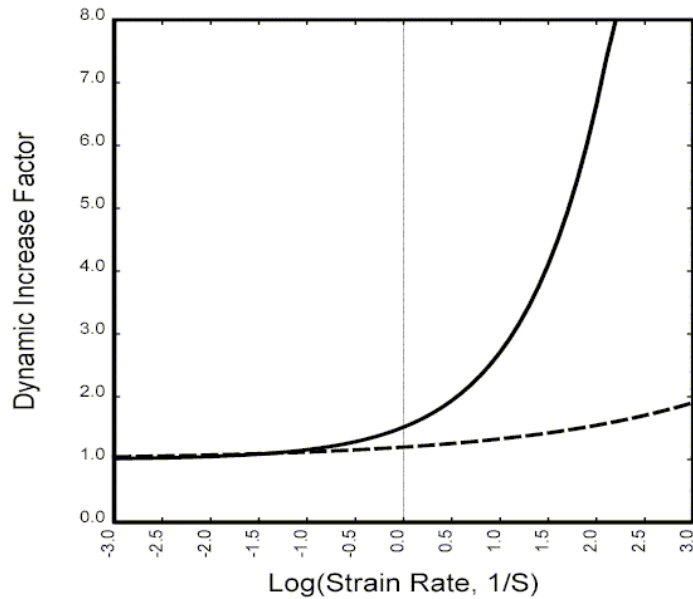
features that can capture the typical behavior of concrete,Figure 4.7.—Tensile and compressive DIF in CSCM with default parameters.

including nonlinear hardening and variation of its strength as a function of confinement. It also contains unique aspects of concrete, including shear dilatation or post-peak stress softening.

The key features of the KCC model include:

- Three-tiered plasticity surfaces
- Hardening that is related by an EOS
- Damage based on a damage evolution input curve
- Rate effects for increasing strength in high strain rate applications
- Confinement effects
- Automated parameter generation scheme based on the uniaxial compressive strength parameter, f'_c (implemented in the third release of the model)

4.2.2   Plasticity Surfaces

The KCC model is based on a three-surface plasticity formulation. It uses stress differences to describe the yield surface, the limit surface and the residual surface. The yield surface, maximum surface, and residual surface are three fixed surfaces defined by the user along with the damage parameters used to determine the appropriate stress state to be used from the three curves. The basic form of this three surface model is portrayed on figure 4.8.

$$\Delta\sigma = \sqrt{3J_2} > 0$$
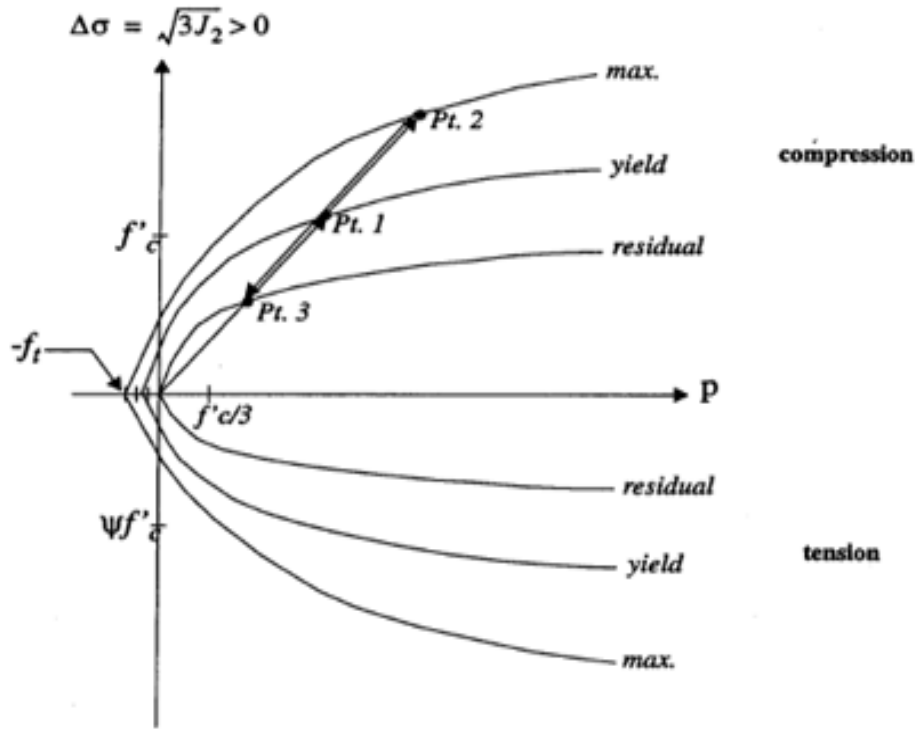
Figure 4.8.—Nested surfaces represented in KCC Model (Mat_72R3) (Malvar et al., 1997).

Eight parameters are used in the KCC Model to define the three fixed surfaces.

$$\Delta\sigma_m = a_0 + \frac{p}{a_1 + a_2\,p} \qquad \text{(maximum failure surface)} \;,$$

$$\Delta\sigma_r = \frac{p}{a_{1f} + a_{2f}\,p} \qquad \text{(residual failure surface)} \;,$$

$$\Delta\sigma_y = a_{0y} + \frac{p}{a_{1y} + a_{2y}\,p} \qquad \text{(yield failure surface)} \;.$$

where $\Delta\sigma_\iota$ is the deviatoric stress invariant, p is a pressure (positive in compression), and a_i are the surface parameters specified by theuser.

The coefficients for the maximum surface are readily found with conventional triaxial test data. Release III, autogeneration, uses the following calculations to find the a_i – coefficients. The coefficients are either fixed values or are a function of the unconfined uniaxial compression strength, f'$_c$:

Table 4.5.—Auto generation parameters for the KCC Model

Curve	Intercept a_0	Parabolic bend coefficient, a_1	Parabolic end point coefficient, a_2
Yield	0.2232 f'$_c$	0.625	0.2575/f'$_c$
Maximum	0.2985 f'$_c$	0.4463	0.0808/f'$_c$
Residual	None	0.4417	0.1183/f'$_c$

4.2.3   Rate Effects

Rate effects are implemented in the KCC Model by expanding and contracting the size of the yield surface in proportion to the magnitude of the strain rate and the dynamic increase factor DIF. DIF is computed from a set of tabular values specified by the user and is different for compression and tension.

Data for tests of typical concrete are shown on figure 4.9. Other supporting data were published by Bishoff and Perry (1991). In this figure, note that there is a predicted difference in tension strain rate effects with the maximum for tension shown as 7.96 and the maximum for compression shown as 3.0. Also note that tension and compression can both be entered in LS-DYNA using a sign convention. It is generally accepted that the ratio of dynamic to static strengths is greater as the strength decreases.

Data from static and dynamic compression tests of dam cores were shown on figures 2.23 and 2.24. If an estimate is made, data on figure 2.24 suggests a 10% increase from the static compressive strength. However, note on figure 2.23 that a static to dynamic ratio needs to be established case by case. There can be a considerable range in values, and the ratio to dynamic values can vary, including the possibility of no increase.

The capacity of the KCC Model to capture the confinement effects is portrayed on figure 4.10.

4.2.4   Softening Parameters

The softening parameters, b_i, establish the manner of softening exhibited by the model for the unconfined uniaxial compression (UUC) and unconfined uniaxial tension (UUT) path stress.
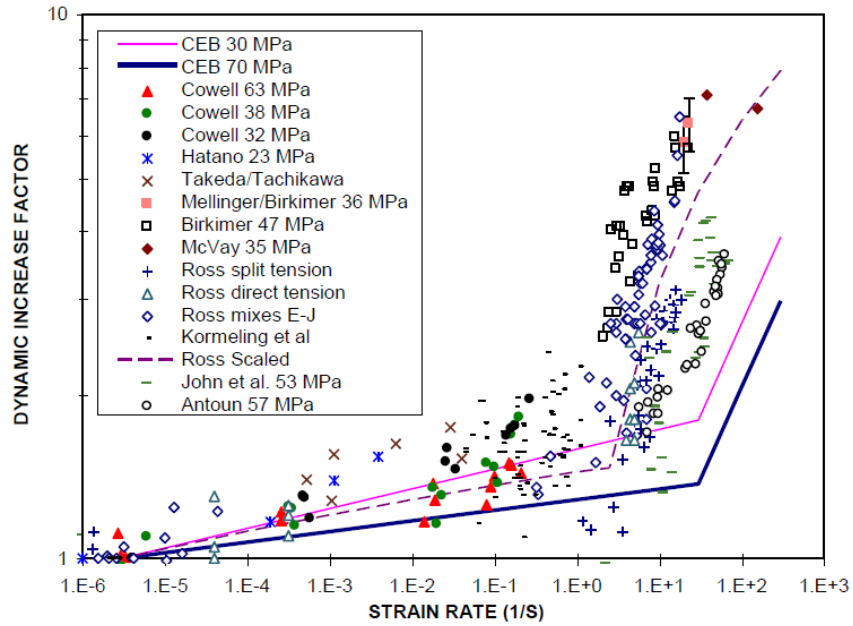
Figure 4.9.—Rate effects data related to concrete strength Bishoff and Perry,1991) confinement effects.
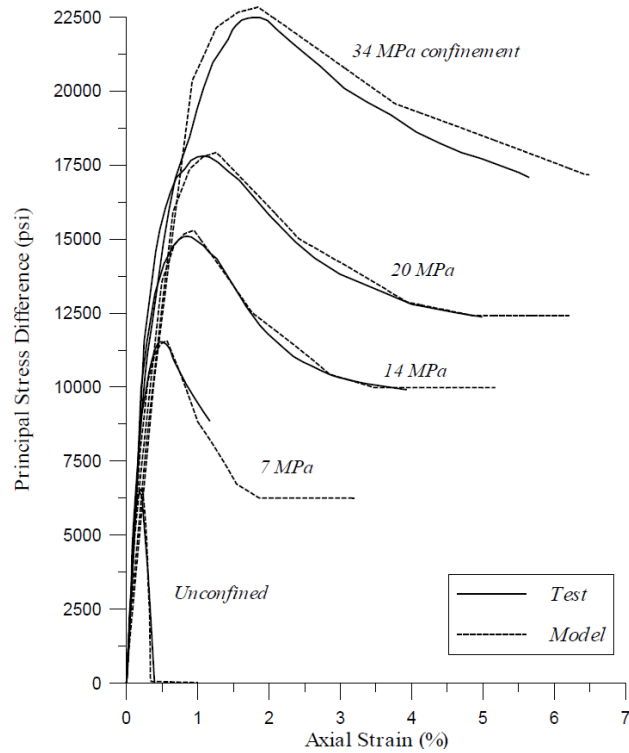
Figure 4.10.—Comparison of measured and predicted results from a TXC test (Malvar et al., 1996).

4.2.5　Elastic Parameters

Two elastic constants are used by the KCC Model, the bulk modulus, K, and Poisson's ratio, v. The shear modulus is computed as:

$$G = \frac{3(1-2v)}{2(1+v)}K'$$

where: K' is the scaled bulk modulus

$$K' = (K_L - K_U)e^{-5.55\varphi} + K_U$$

where K_U and K_L are the unloading and loading bulk modulus, respectively. Parameter φ is calculated by:

$$\varphi = \frac{\Delta\varepsilon}{\Delta\varepsilon - (p - p_f)/K_U}$$

where p_f is the intersection of the residual surface with the pressure axis and is equal to zero for concrete, and $\Delta\varepsilon$ is a change of volumetric strains.

4.2.6　Damage Function

The three fixed surfaces are used to define the dynamic form of yield surface that is obtained by interpolation between the yield surface and the maximum failure surface during hardening and between the maximum and residual surfaces during softening. The interpolation is obtained using a damage parameter λ.

After the stress point reaches the yield surface, but before approaching the maximum surface, the current surface is obtained as a linear interpolation between the two as:

$$\Delta\sigma = \eta(\Delta\sigma_m - \Delta\sigma_y) + \Delta\sigma_y$$

To determine the selection and use of the three failure surfaces, a function with a nondecreasing damage parameter, λ- η , is used. The value η is chosen from a function related to a nondecreasing damage parameter, λ. The values of η start at 0 and increase in sequence to 1. After reaching the maximum values, the current failure surface is similarly interpolated for unloading between the maximum and the residual surfaces as:

$$\Delta\sigma = \eta(\Delta\sigma_m - \Delta\sigma_r) + \Delta\sigma_r$$

The function for $\eta(\lambda)$ is input as a series of exactly 13 pairs. Two datasets are available for this input based on previous testing values. The White Sands Missile Range (WSMR) data are from WSMR testing (Joy and Moxley, 1993),

and the Strategic Air Command data are from the Air Force Civil Engineering Laboratory for the Strategic Air Command (Ross et al., 1992). This input can be autogenerated when that feature is activated.

The plastic strains are adjusted by r_f – the rate enhancement factor, s – the lambda stretch factor, and b_1 and b_2 – damage scaling coefficients. Accounting for these extra parameters, the damage parameter, λ, is expressed as:

For positive pressures:

$$d\lambda = d\epsilon^p / \ [(1+(s/100)(r_f-1)](1+p/r_f\,f_t\,)^{b}{}_1$$

and for negative pressures:

$$d\lambda = d\epsilon^p / \ [(1+(s/100)(r_f-1)](1+p/r_f\,f_t\,)^{b}{}_2$$

Note that if s = 0, rate effects are eliminated in the damage calculation. With s = 100, 100% of the rate effect is used. Thus, s is a percentage of the rate effect to be used.

With damage as described above, if an isotropic tension test is modeled wherein the pressure decreases from 0 to $-f_t$ with no deviators, then no damage would occur. The parameters λ and η would both remain 0.0. The EOS would decrease the pressure to $-f_t$ and keep this value thereafter. To implement a pressure decay after tensile failure, a volumetric damage increment is added when the deviatoric damage is along the negative hydrostatic axis. This factor is 1.5 for the biaxial (splitting) tension test. To limit the effects of this change to the paths close to the triaxial tension path, the incremental damage is multiplied by a factor, f_d, given by:

$$f_d \ = \ |(3J_2)^{1/2}/p\,|\,/0.1 \quad \text{for} \quad |(3J_2)^{1/2}/p\,| \ < 0.1$$
$$0 \quad \text{for} \quad |(3J_2)^{1/2}/p\,| \ >= 0.1$$

The modified effective plastic strain is incremented by

$$d\lambda = b_3\,f_d\ k_d\,(\epsilon_v - \epsilon_{v\,\text{at yield}})$$

where b_3 is an input variable, k_d is an internal variable, and ϵ_v is volumetric strain.

There are no direct data for b_3, but the authors of the model suggest a value between 1.1 and 1.6.

In LS-DYNA, the material strength of the elements is reduced to values given by the residual curve when the damage parameter approaches a value of 2.0.

4.2.7   Shear Dilation

Shear dilation is included in the KCC model. Dilatancy in this sense is the effect of sliding surfaces needing to clear jagged planes created by aggregate extrusions into the plane (figure 4.11). Once the gap is sufficiently open to clear these jagged peaks, the dilatancy no longer occurs. A factor, w, is used to vary this effect. This parameter can be reasonably estimated, and typical concrete experiments show it to be between 0.5 and 0.7. The value of the parameter ranges from 0, which implies no change in volume during plastic flow, to 1, which implies shear dilation during flow. The dilatancy decay can also be controlled by the parameter, *edrop*, which varies from 1 (a linear drop to 0), to a large number (a rapid drop).
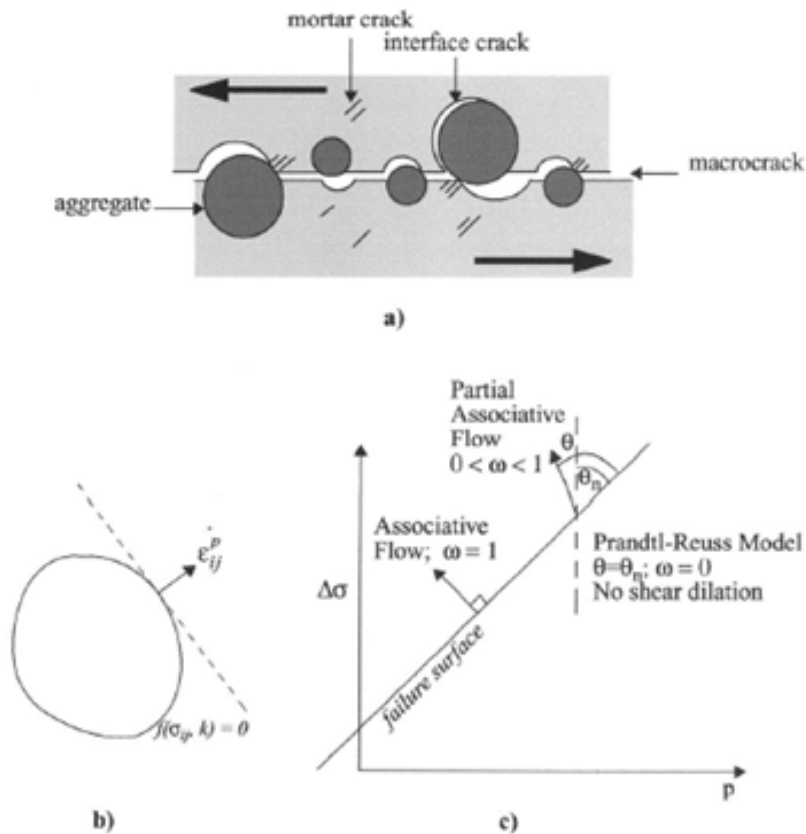
**Figure 4.11.—Shear dilatancy. a) Graphical representation of
shear dilatation, b) yield surface with associated flow rule,
and c) description of associative, nonassociative, and partial
flow rules (Malvar et.al, 1996).**

4.2.8   Equation of State

The EOS is input as a (piecewise linear) table of values of volumetric strain versus pressure, temperature (not generally used in dam analysis), and bulk modulus (figure 4.12). Unload/reload tests are required to find the bulk modulus at varying values of pressure and volumetric strain as previously mentioned in section 3.0. Complete data from lab testing are seen on figure 4.13, showing axial and lateral strains. Note that actual data patterns match the assumed behavior. Measured lateral strains are large at higher stresses, showing the bulging of the cylinder as it fails.
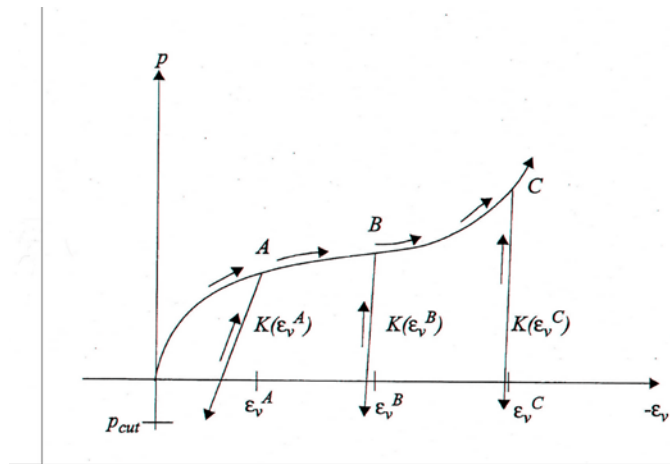
Figure 4.12.—EOS for the KCC Model (Malvar et al., 1996).

Poisson's ratio is input as a scalar parameter. Generally, this value is calculated from the initial stress-strain values as an elastic value.

4.2.9   Erosion of Elements

The KCC model does not have an in-built erosion and crack simulating mechanism. In order to simulate the physical cracks in concrete, an external erosion algorithm called "Mat_Add_Erosion" needs to be implemented. This LS-DYNA feature is based on the concept that the element is deleted when the material response in an element reaches certain criteria.

4.2.10   Default Parameters

The KCC model provides the capacity to generate a fit for different concrete strengths by using f'$_c$ to vary the autogenerated parameters required for analysis. The fit is based on data the K&C obtained for a specific type of concrete

Black Canyon Dam: DH-05-2 29.3-30.21
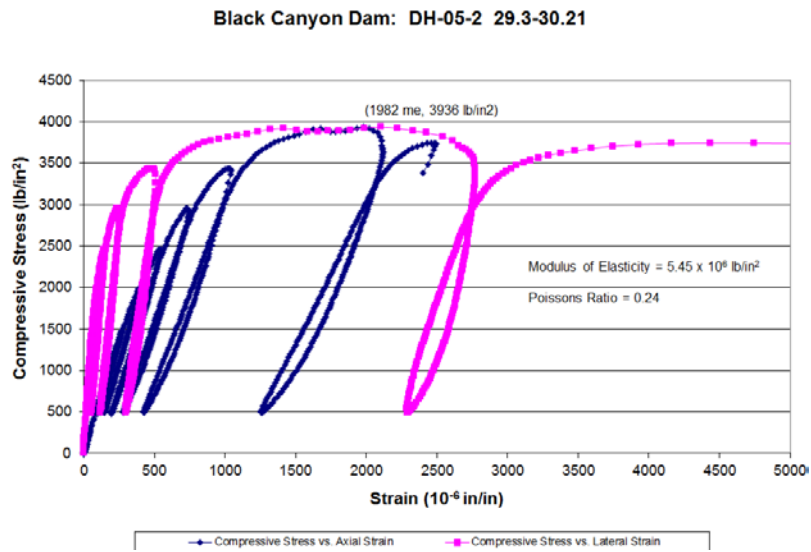
**Figure 4.13.—Black Canyon lab testing data showing unload/
reload data (Madera, 2005).**

designated here as KC-concrete (f'$_c$ = 6,580 psi.). The default values of the KCC
model were derived using LS-DYNA to fit the model to the KC-concrete data.
These values are listed in table 4.6.

Table 4.6.—Default parameter values used by the KCC Model

Parameters			Parameter Values Used
Category	Symbol	Description	LS-DYNA Defaults
1: surfaces	a_{0y}	Yield surface	1469 psi
	a_{1y}	Yield surface	0.625
	a_{2y}	Yield surface	3.913E-5 /psi
	a_{0m}	Max surface	1,945 psi
	a_{1m}	Max surface	0.4463
	a_{2m}	Max surface	1.228E-5 /psi
	a_{1r}	Residual surface	0.447
	a_{2r}	Residual surface	1.797E-5 /psi
2: softening	b_1	Compression softening[2]	1.6
	b_2	Tensile softening	1.35
	b_3	Volumetric extension softening	1.15
3: damage evolution	λ_1, η_1	Damage function is specified using 13 points to define η as function of the damage parameter λ. The λ parameter is computed from the state variables at a material point and is updated at every step of the analysis.	0.0, 0.0
	λ_2, η_2		0.8E-5, 0.85
	λ_3, η_3		2.4E-5, 0.97
	λ_4, η_4		4E-5, 0.99
	λ_5, η_5		5.6E-5, 1.00
	λ_6, η_6		7.2E-5, 0.99
	λ_7, η_7		8.8E-5, 0.97
	λ_8, η_8		32E-5, 0.5
	λ_9, η_9		52E-5, 0.1
	λ_{10}, η_{10}		57E-5, 0
	λ_{11}, η_{11}		1.0, 0
	λ_{12}, η_{12}		10.0, 0
	λ_{13}, η_{13}		1.0E10, 0
4: properties	f_c'	Concrete strength	6,580 psi
	f_t	Tensile strength	554 psi
	K	Bulk modulus	Provided by the EOS
	ν	Poisson's ratio	0.19
	G	Shear modulus	Computed using K and ν
	ρ	Density	145 pcf, 2.172E-4 lbs-sec^2/in^4
	ω	Shear-dilatancy factor	0.5
	W	Localization width due to aggregate size[1]	0.375 inch

Note: W is set to three times the aggregate size.

5.0 SINGLE ELEMENT SIMULATION

Both the KCC model and the CSCM are evaluated here using a single element to verify the performance of concrete models and to display the basic stress-strain relations.

5.1 Description of Single Element Model

Uniaxial tension and compression of a single element were simulated for three different concrete strengths, f'$_c$, (3,200 psi, 4,350 psi, and 6,500 psi) and appraised based on the data from Black Canyon Dam cores tested using conventional triaxial methods. The material input parameters were automatically generated for both the KCC model and the CSCM, which were developed for concrete mixtures with only 3/4-inch aggregate, while the NMSA in Black Canyon Dam is 6-inches. The analysis of a 2-inch concrete cube was conducted with single cubic hex elements H1, H2, and H3, shown on figure 5.1. The size of each element is 1 inch in each dimension, assuming the triple symmetry of the cube.
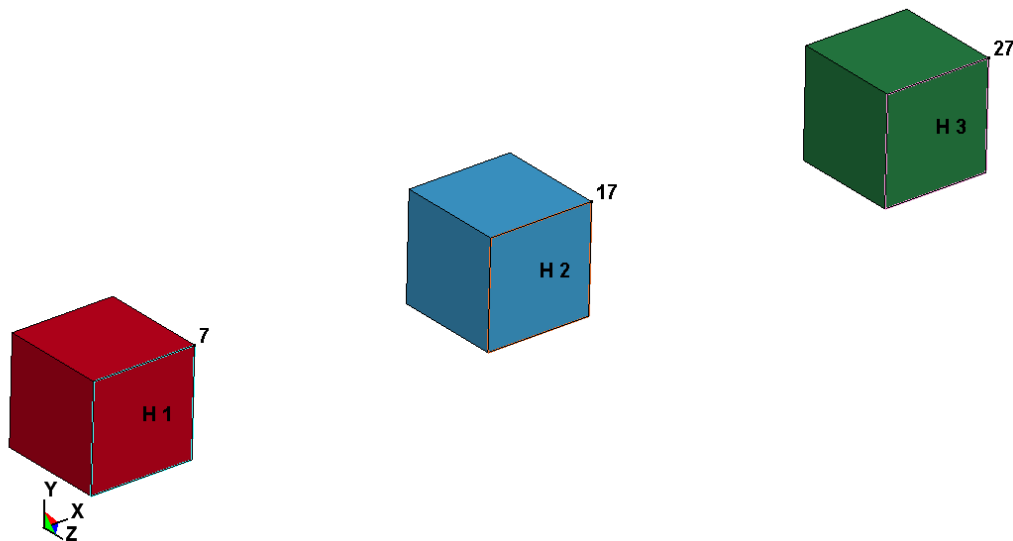
Figure 5.1.—Single element used for simulation of the KCC Model and CSCM with the strength of material assigned to elements as H1 = 3,200 psi, H2 = 4,350 psi, and H3 = 6,500 psi.

5.2 Results for CSCM Material Model Analysis

The analysis was performed with model autogenerated parameters for the concrete strength of 3,200 psi, 4,350 psi, and 6,500 psi and the maximum

aggregate size of 3/4 inch. It should be noted that the plastic hardening effect is not included in the default setup of CSCM parameters. The stress-strain relations obtained in the analysis for compression and tensions are presented on figure 5.2, with the failure strength and corresponding strains listed in table 5.1.
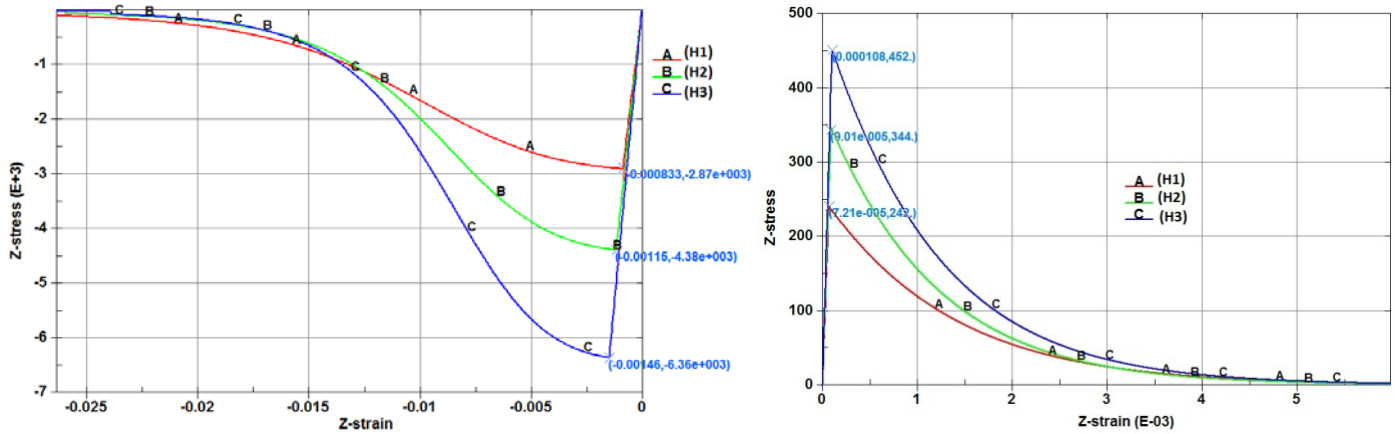
Figure 5.2.—Strain-stress results for single element using the CSCM without hardening for UUC (left) and UUT (right) with curves A, B, and C corresponding to elements H1, H2, and H3, respectively.

Table 5.1.—Results for single element simulation in UUC and UUT (stresses in [psi])

Test No. (Concrete Strength)	Initial Elastic Modulus in Compression	Strain at Failure in Compression	Compression Strength	Strain at Failure in Tension	Tension Strength
H1 (3,200)	3,450,000	-0.00084	-2,890	0.00007	242
H2 (4,350)	3,810,000	-0.00115	-4,380	0.00009	344
H3 (6,500)	4,370,000	-0.00145	-6,360	0.00010	452

5.3   KCC Model Analysis Results

Figure 5.3 shows the KCC single element model results, with table 5.2 detailing the results.
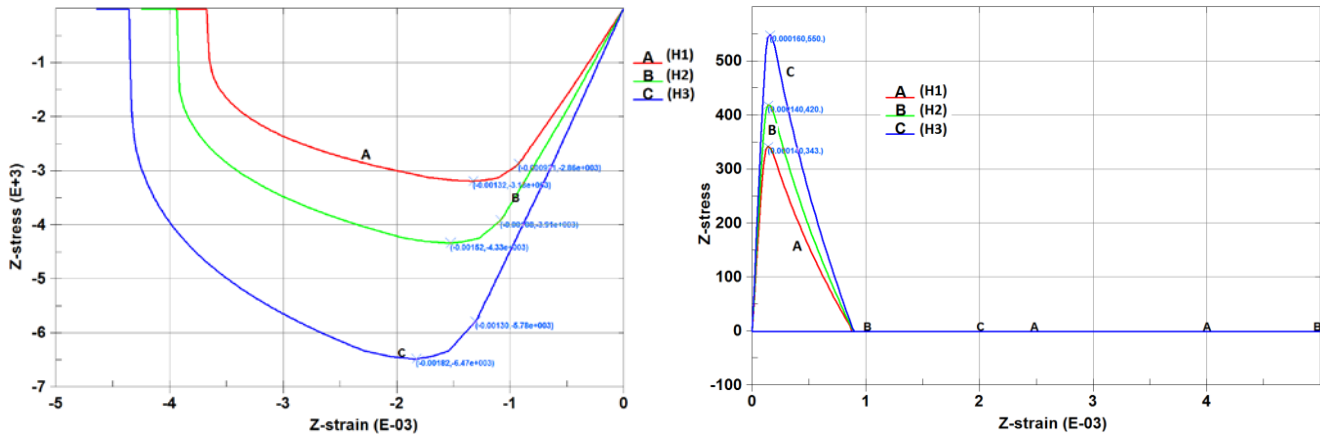
Figure 5.3.—Strain-stress results for single element using KCC Model for UUC (left) and UUT (right) with curves A, B, and C corresponding to elements H1, H2, and H3, respectively.

Table 5.2.—Results for single element simulation in UUC and UTT (stresses in [psi])

UCC			
Test No. (Concrete Strength)	**Initial Elastic Modulus in Compression**	**Strain at Failure in Compression**	**Compression Strength**
H1 (3,200)	3,108,000	-0.00132	-3,200
H2 (4,350)	3,620,000	-0.00152	-4,350
H3 (6,500)	4,446,000	-0.00182	-6,500
UUT			
Test No. (Concrete Strength)	**Initial Elastic Modulus in Tension**	**Strain at Failure in Tension**	**Tension Strength**
H1 (3,200)	3,080,000	0.00014	343
H2 (4,350)	3,610,000	0.00014	420
H3 (6,500)	4,350,000	0.00016	550

5.4   Observations

The following observations have been made based on the single element analysis for CSCM and KCC model:

- For the CSCM, the compressive strength values vary slightly from the input values, using the default fitting parameters, but are reasonable values. Tensile strength and strains in compression and tension are reasonable.

- For the KCC model, compressive strength values match the input values using the default fitting parameters. Tensile strength and strains in compression and tension are reasonable.

- The CSCM produces failure strains lower than the KCC model for both compression and tension. The stress-strain relationship in tension is linear.

- The CSCM produces tensile strengths of the order of 7% of the compressive strength; the KCC model produces tension strengths on the order of 8% of the compressive strength. The lower value is closer to measured data, which are approximately 4.5% (see figure 2.17), but both are within the range of measured values.

6.0 CONCRETE CYLINDER COMPRESSION TEST SIMULATION

6.1 Simulation of TXC Test

Numerical simulation of a uniaxial compression (UXC) test is presented in this section. The CSCM was used to model a 6-inch diameter by 12-inch long concrete cylinder compressed by two steel bearing plates. Contact with various coefficients of friction was introduced between the concrete sample and the steel bearing plates (figure 6.1). The bottom bearing plate was fixed, but the upper plate moved at various rates of speed.
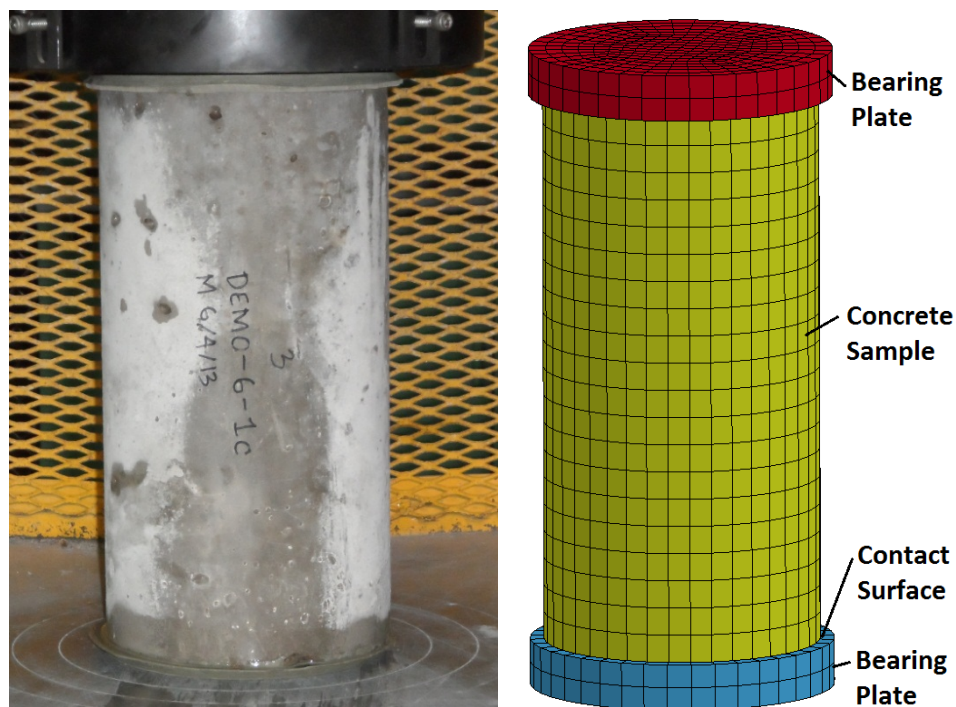

Figure 6.1.—UXC test (left) and the corresponding FE model.

The simulation was conducted for three different concrete strengths, f'_c: 3,200 psi, 4,350 psi, and 6,500 psi. Default CSCM material model parameters were assumed in the analysis. The load rate effect and various friction conditions between the concrete and the steel bearing plates are being investigated.

6.2   Analysis Results

A failed cylinder is shown on figure 6.2 for comparison to results that follow. Note the pointed cone nature of the failure with an intact ring near the fixed, lower end. The ability to model the development of the shear failure surfaces is a key comparison for model results. Other numerical comparisons are also made in the following sections.

Figure 6.2.—Geometry typical of a failed cylinder from UXC Unconfined Test
(Photo by Harris; courtesy of Materials Engineering and Research Laboratory)

6.2.1   Stresses and Deformation in UXC Sample

Figure 6.3 shows maximum shear stresses, von Mises stresses, and vertical stresses from the simulation. The shear and von Mises stresses show the failure mechanism typical in actual failures. The vertical stresses show high values in the outer diameter of the more central two-thirds of the cylinder also representing the region that will barrel out as the cylinder fails. Figure 6.4 clearly shows displacements of the sections barreling away from the cylinder. The damage zone also indicates the development of the failed cylinder compared to the actual test as shown on figure 6.1. Thus, multiple calculated parameters can be used to indicate failed conditions.

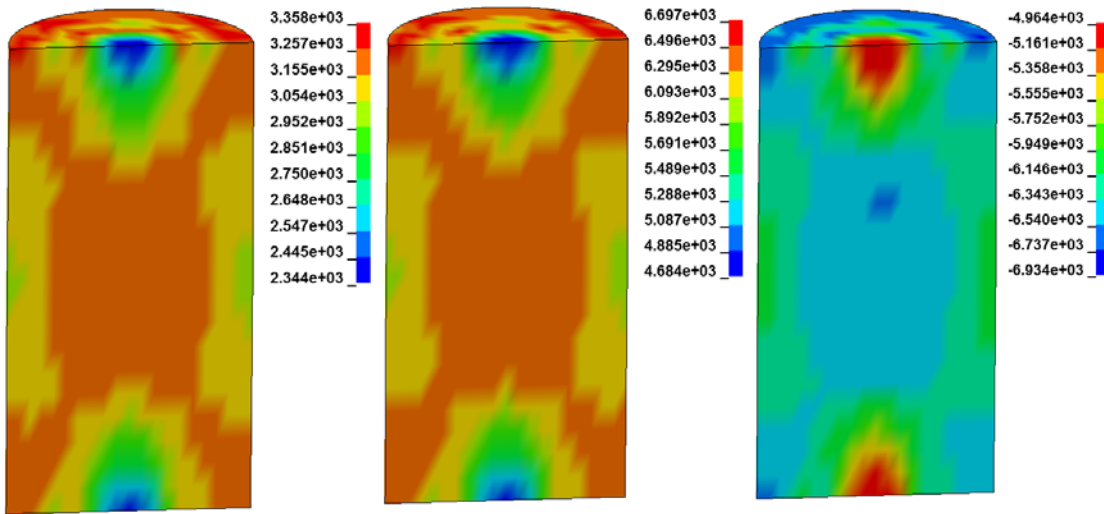**Figure 6.3.—Maximum shear stress (left), Von Mises stress (center), and vertical stress (right) at 0.06 inch piston movement for 6,500 psi concrete.**
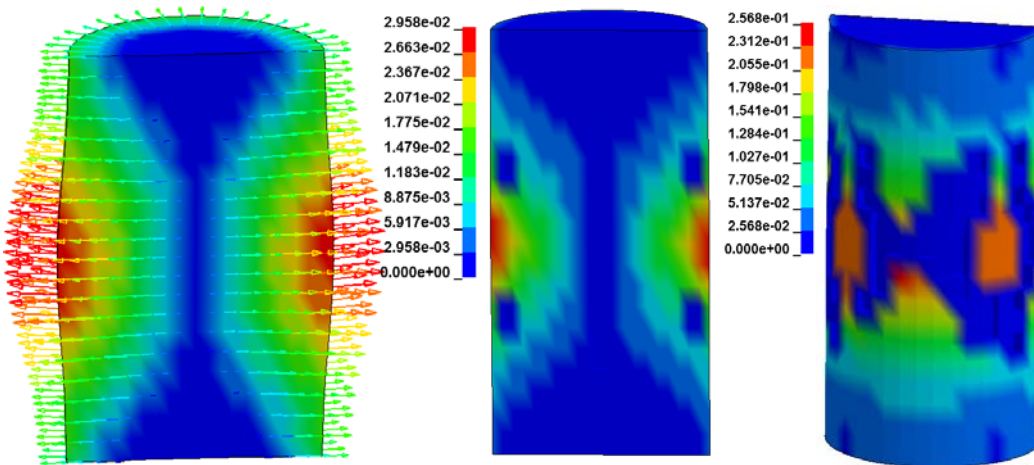
Figure 6.4.—Lateral displacement at 0.06 inch piston movement (left) and lateral displacements at 0.3 inch piston movement with shown concrete damage inside the sample (center) and at the outside (right) for 6,500 psi concrete.

6.2.2 Compression Force in UXC Test

Figure 6.5 shows the relationship between the piston movement and the force in the piston for three concrete strengths. The maximum force calculated is provided in table 6.1.
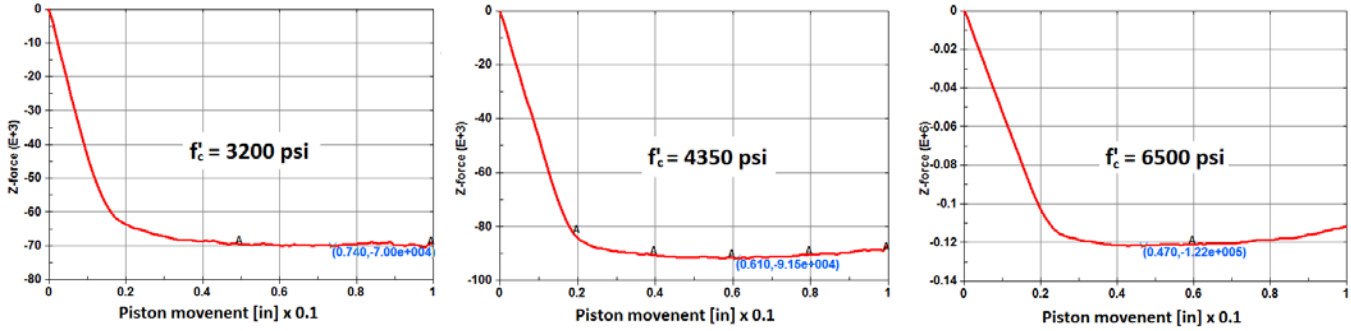
Figure 6.5.—FE analysis compression force as a function of piston movement.

Table 6.1.—UXC results for 6-inch-diameter specimen (rate effect not included) per figure 6.2

Material Model and (Strength [psi]) (1)	Calculated Maximum Force [lbf] (2)	Stress at Maximum Force [psi] (3)	Difference (4)	Concrete Strength per the Test (5)
H1 (3,200)	-70,000	-2,475	23.6 %	2,500
H2 (4,350)	-91,500	-3,235	25.6%	3,200
H3 (6,500)	-122,000	-4,315	33.6%	4,300

Results from table 6.1 demonstrate significant differences between the specified concrete strength for material models (column 1) and the actual concrete strength obtained in the UXC test (column 5). This simple test demonstrates that using the single parameter input for autogeneration of parameters needs to be considered as a strength coefficient, $f'_c{}^*$, not as a direct input of compressive strength.

6.2.3 Confined Compression Test

The TXC simulation was performed for confined pressure at 50 psi and 150 psi. The results of the analysis are provided in table 6.2. The analysis demonstrated the importance of the biaxial load effect on the strength of the concrete.

Table 6.2.—TXC results for 6-inch-diameter specimen for various confined pressure

Material Model Strength [psi] (1)	Confined Pressure [psi] (2)	Calculated Maximum Force [lbf] (3)	Stress at Maximum Force [psi] (4)	Difference (5)
H1 (3,200)	0	-70,000	-2,475	-
	50	-75,700	-2,678	7.6%
	150	-85,000	-3,007	21.5%

6.2.4   Load Rate Effect

A strain load rate of 10^{-3} was applied to the cylinder loading to demonstrate the effect of this parameter. Results are shown on figure 6.6 with an increased load ratio of 1.1 with the strain rate increase. This increase is consistent with published laboratory test values (Harris et al., 2000).
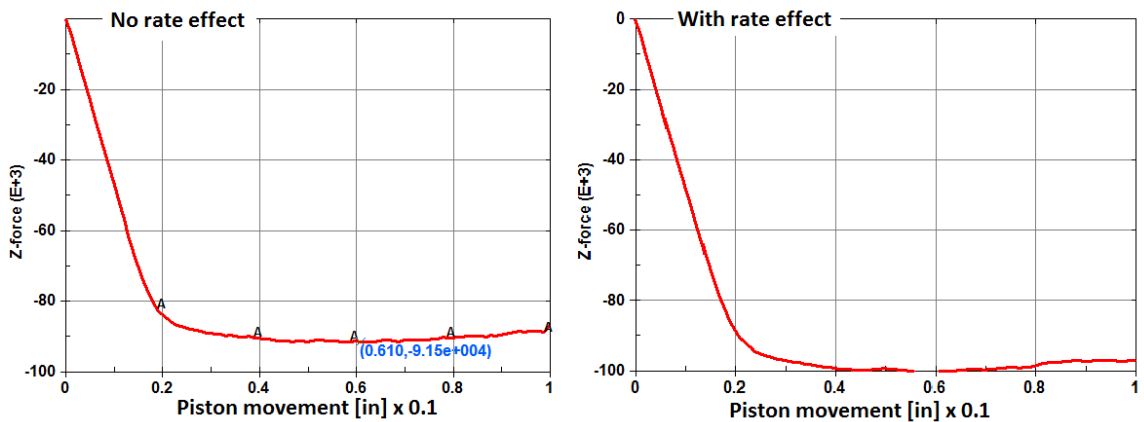
Figure 6.6.—Test with no load effect (left) and with the effect (right) for piston movement at 0.1 inch per second.

6.3   Observations

Values for the predicted compressive stress failures for the single element and cylinder simulations are tabulated together in table 6.3. The table shows greater differences for the cylinder simulation. The single element case is stronger, as the boundary conditions produce an effect similar to confinement. The cylinder simulation is recommended as a "patch" test for verification of the input parameter $f'_c{}^*$ to assure that the coefficient generates desired strengths in the analysis. The uniaxial model can be used to confirm measured laboratory test

Table 6.3.—TXC results for computer model strength tests (rate effect not included)

Material Model & (Input Generation Value [psi]) (1)	Calculated Failure Value sinlge element (2)	Calculated Failure Value Cylinder Test [psi] (3)	Difference 1 element (4)	Difference Cylinder (5)
H1 (3,200)	-2,900	-2,500	10 %	24%
H2 (4,350)	-4,400	-3,200	1%	26%
H3 (6,500)	-6,400	-4,300	1%	34%

values. Runs will be iterated as necessary to produce agreement between the lab results and the analysis results. The 50-psi confining pressure model should be considered for areas deep inside a dam where confining effects will be present.

The results from rate effect in the models agree with previously published laboratory results. This parameter can be used as demonstrated in this study.

7.0   SUMMARY AND CONCLUSIONS

7.1   Summary

The following observations are made based on the study in this report:

The CSCM constitutive material model was implemented for analysis of mass concrete for dams. The model is capable of simulating the characteristics of conventional mass concrete that include:

- Plasticity-damage based softening with erosion and modulus reduction
- Rate effect for increasing strength in high-strain rate applications
- A hardening cap that expands and contracts

The study showed that the Continuous Surface Cap Model for concrete is effective and efficient and could be used in the nonlinear analysis of concrete dams for Dam Safety Office projects.

Both single element simulations and a "patch" test using a compression test of a cylinder show differences from the CSCM auto-generation parameter and the resulting failure stress. Use of auto-generation should consider the parameter as $f'_c{}^*$, where iterations of this parameter can be done with the patch test to confirm that the desired failure stress will be achieved.

The CSCM generates tensile strengths on the order of 7%, which generally agrees with values from laboratory samples of approximately 5%.

The CSCM accurately predicted failure in a cylinder, showing the same failure mechanism as is typical in laboratory tested cylinders. Multiple parameters are available – all of which correctly indicated failure conditions.

In general, strain rate modifications in strength using the CSCM agree with published results.

Concrete used in dams and conventional concrete used in structures have different properties. Laboratory measured modulus values vary from ACI and CEB recommended estimating equations for modulus. Strain values at maximum stress for laboratory measured values are on the order of one-half of the recommended ACI 318 values for design. Values of compressive strength show a large range for a set of tests from cored materials. Tensile strength to compressive strength ratios are in the 5–7% range.

The calibration study for KCC model showed that MAT_72R3 has numerical problems in the most current LS-DYNA version used in the evaluation. The Livermore Software Technology Corporation technical support confirmed our concerns, stating that the observed issues will be corrected in the new MAT_72R4

release. Considering deficiency of the KCC model in LS-DYNA, this report presents the theoretical basis of the model and the results of simulation for single element only.

7.2 Conclusions

The following are conclusions derived from the investigations:

- The CSCM appears to be a reliable tool for modeling the nonlinear behavior and failure conditions in concrete materials for dams.

- Based on the results included in this report, it is recommended that the CSCM is included in the state of practice for the nonlinear analysis of concrete dams for Dam Safety Office projects.

- The results of this study showed that the K&C Mat_72R3 material model, used currently in the nonlinear analysis of concrete dams, has numerical issues. It is recommended that the model not be used until the new R4 release of the KCC model is implemented in LS-DYNA software.

8.0 REFERENCES

Abrams, Duff, A., 1918, "Design of Concrete Mixtures," Structural Materials
    Research

American Concrete Institute (ACI) Committee 207.1R-05. 2005, – Mass and
    Thermally Controlled Concrete.

American Concrete Institute (ACI) Committee 318, 2011, ACI 318-11, Building
    Code Requirements for Structural Concrete and Commentary.

Anderson, C, C. Mohorovic, L. Mogck, B. Cohen, and G. Scott, 1998, "Concrete
    Dams Case Histories of Failures and Nonfailures with Back Calculations,"
    DSO-98-05, Bureau of Reclamation.

American Society for Testing and Materials (ASTM) International, 2009, Annual
    Book of ASTM Standards, West Conshohocken, PA.

Attard, M.M. and S. Setunge, 1996, "Stress-Strain Relationship of Confined and
    Unconfined Concrete," ACI Materials Journal, September–October 1996.

Bazant, Z.P. and J. Planas, 1997, Fracture and Size Effect in Concrete and Other
    Quasibrittle Materials, CRC Press, New York.

Bishoff, P.H. and S.H. Perry, 1991, "Compressive Behavior of Concrete at High
    Strain Rates," Materials and Structures, Vol. 24, pp. 425–450.

Bureau of Reclamation (Reclamation), 1949, Boulder Canyon Project Final
    Reports, Part VII – Cement and Concrete Investigations, Bulletin 2,
    Investigations of Portland Cements, Bureau of Reclamation, Denver,
    Colorado.

_____, 1992, Concrete Manual, Part 2 (Ninth edition).

_____, 2006, Computer Material Models for Soils using FLAC and DYNA,
    Bureau of Reclamation, Dam Safety Technology Development Program,
    Denver, Colorado.

Comité Euro-International du Béton (CEB), 1993, CEB-FIP Model Code, 1990,
    Comité Euro-International du Béton, Thomas Telford House, Červenka,
    January (1990) "Discrete Crack Modelling in Concrete Structures," Ph.D.
    thesis, University of Colorado, Boulder.

Davis, Raymond E., H.E. Davis, and J.W. Kelly, (about 1932), "Bonding of
    New Concrete to Old at Horizontal Construction Joints," Concrete
    Laboratory file 390.7.5.

Dolen, T.P., 2005, "Parker Dam – 2005 Concrete Coring – Laboratory Testing Program," Bureau of Reclamation, Technical Report MERL-2005-20.

_____, 2010, "Advances in Mass Concrete Technology – The Hoover Dam Studies," Hoover Dam 75th Anniversary Symposium, ASCE.

Dolen, T.P., D.W. Harris, and L.K. Nuss, 2014, "Tension Strength of Mass Concrete – Implications of Test Procedures and Size Effects on Structural Analysis of Concrete Dams," United States Society on Dams, 34th Annual Meeting and Conference, held April 7–11, 2014, San Francisco, CA.

Harris, D.W., C.E. Mohorovic, and T.P. Dolen, 2000, "Dynamic Properties of Mass Concrete Obtained from Dam Cores," ASCI Materials Journal, Vol. 97, No. 3.

Harris, D., 2006, "Computer Material Models for Soil, Rock, and Concrete using FLAC and DYNA," DSO-06-01, Bureau of Reclamation.

Joy, S. and R. Moxley, 1993, "White Sands Missile Range 5-1/4 inch Concrete Properties," United States Army Corps of Engineers Briefing, prepared for the Defense Special Weapons Agency, distribution limited to Government agencies and their contractors, critical technology.

Madera, V., "2005, Concrete Coring – Laboratory Testing Program, Black Canyon Dam," Technical Memorandum Number MERL 05-11, Bureau of Reclamation.

Malvar L.J., J.E. Crawford, J.W. Wesevich, and D. Simons, 1994, "A New Concrete Material Model for DYNA3D," Report No. TM-94-14.3

Malvar L.J., J.E. Crawford, J.W. Wesevich, and D. Simons, 1996, "A New Concrete Material Model for DYNA3D – Release II: Shear Dilation and Directional Rate Enhancements," Report No. TM-96-2.2

_____, 1997, "A Plasticity Concrete Material Model for DYNA3D," Intl. J. Impact Engr., Elseveir Publishing, Great Britain.

Malvar, L.J. and C.A. Ross, 1998, "Review of Static and Dynamic Properties of Concrete in Tension," ACI Materials Journal, Vol. 95, No. 6.

Murray, Y.D., 2007, User's Manual for LS-DYNA Concrete Material Model 159, Aptek, Inc., FHWA HRT-05-062.

Ross, C.A., S.T. Kuennen, and J.W. Tedesco, 1992, "Effects of Strain Rate on Concrete Strength," Session on concrete research in the Federal Government, ACI Spring Convention, Washington, D.C.

Simo, J.C. and J.W. Ju, 1987a, "Strain- and Stress-based Continuum Damage
Models – I Formulation," Int. J. Solids Structures, Vol. 23, No.7,
pp. 821–840.

_____, 1987b, "Strain- and Stress-based Continuum Damage Models – II
Computational Aspects," Int. J. Solids Structures, Vol. 23, No.7,
pp. 841–869.

Timoshenko, S.P. and J.N. Goodier, 1970, Theory of Elasticity, 3rd Edition,
McGraw-Hill Book Company, St. Louis.

ATTACHMENT A

Detailed Data for Black Canyon Dam

Triaxial data for the Black Canyon Dam are shown below. Following the data table is a Mohr-Coulomb diagram showing the data. In this figure, the higher phi angle at lower confining stresses is shown with a lower phi angle at higher confining stresses. Following the Mohr's circle diagram is the construction of a failure surface typical for nonlinear models – in this case, a curve of mean pressure versus deviator stress.

Table A-1.—Detailed triaxial testing data for Black Canyon Dam (Madera, 2005)

Table 4 – Results of Triaxial Compressive Strength Tests on NX-Size Cores from Black Canyon Dam, Cored in 1951, 75 percent saturated moisture content

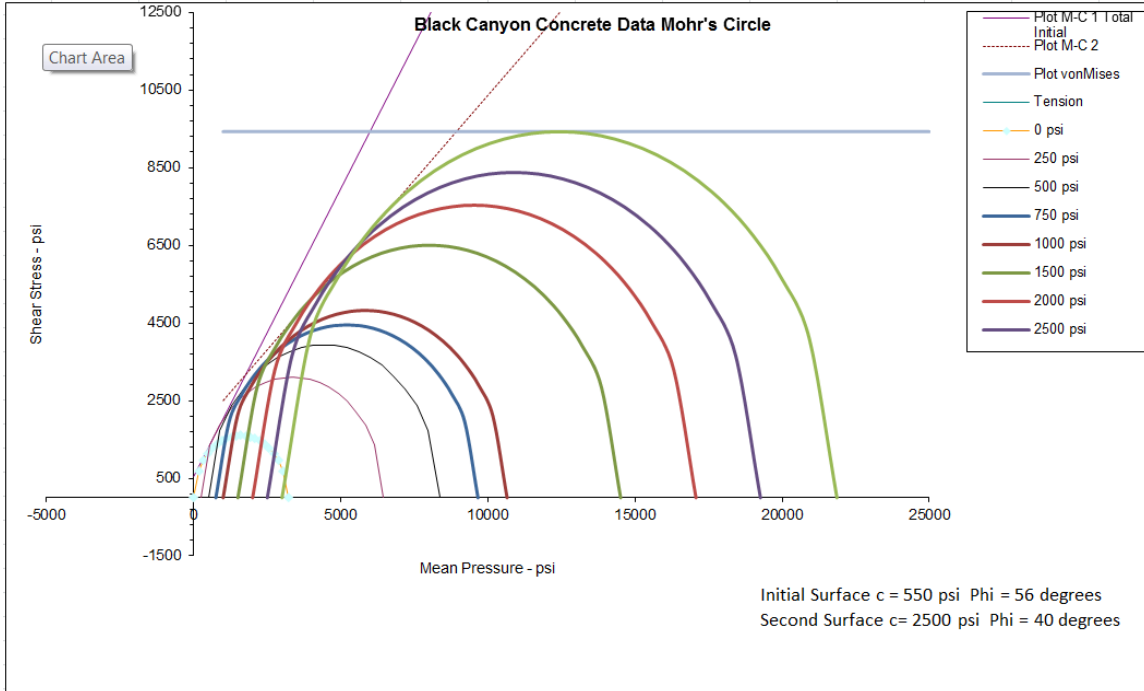| Drill Hole | Depth, ft | | Lateral Stress | Axial Stress | Average Axial |
Station	Top	Bottom	σ_3, lb/in^2	σ_1, lb/in^2	Stress, lb/in^2
1+50	8.0	8.5		2,460	
4+85	5.5	6.3		2,480	
5+78	5.2	5.7	0	3,290	3,200
0+90	7.0	7.9		3,810	
4+46	7.5	8.1		3,970	
1+40	4.8	5.7		4,590	
1+30	5.0	6.2		5,100	
4+88	5.3	6.2	250	5,930	6,210
5+28	5.0	6.2		7,580	
0+70	5.0	6.5		7,640	
5+18	7.4	8.4		6,490	
6+48	8.5	9.6		6,950	
0+80	6.5	7.2	500	7,200	7,870
1+10	4.9	6.2		9,160	
0+70	5.0	6.5		9,550	
5+98	8.3	9.2		7,900	
4+88	5.3	6.2		8,240	
5+18	7.4	8.4	750	8,530	8,810
1+00	6.2	7.1		8,560	
1+10	6.4	7.5		10,800	
5+48	5.4	6.4		7,320	
1+00	6.2	7.1		8,330	
1+00	7.2	8.0	1000	9,800	9,630
1+10	4.9	6.2		11,030	
1+20	5.2	5.8		11,660	
5+68	6.4	7.0		11,410	
1+30	5.0	6.2		11,980	
5+68	5.4	6.4	1500	12,710	13,010
5+28	8.2	9.3		13,370	
5+08	8.0	8.8		15,590	
5+68	5.4	6.4		14,730	
5+28	8.2	9.3		15,340	
6+08	6.0	6.6	2000	15,720	15,740
1+30	5.0	6.2		15,980	
1+40	4.8	5.7		16,910	
5+98	8.3	9.2		15,070	
5+58	8.0	9.0		16,810	
5+48	5.4	6.4	2500	17,070	16,760
5+88	6.4	7.0		17,370	
1+10	6.4	7.5		17,490	
0+70	5.0	6.5		16,070	
1+40	9.0	9.9		16,390	
6+48	8.5	9.6	3000	18,090	18,860
5+58	8.0	9.0		21,330	
5+28	5.0	6.2		22,420	

Figure A-1.—Mohr-Coulomb diagram of Black Canyon Dam triaxial data.
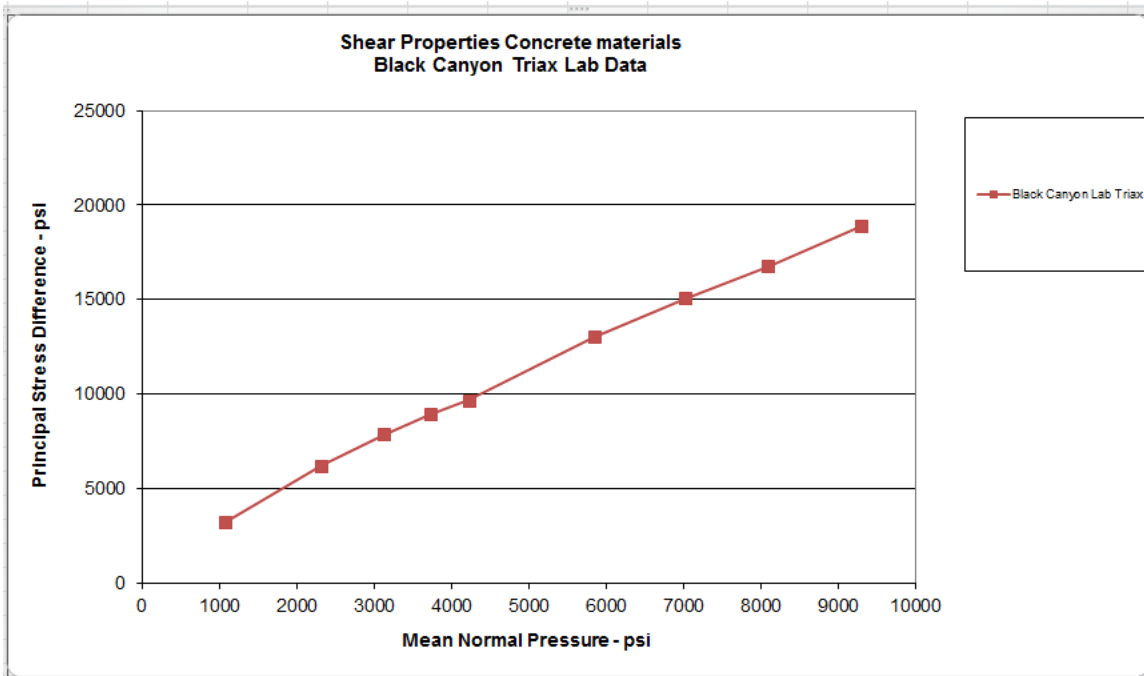(Data compiled by Harris; data courtesy of Materials Engineering and Research Laboratory)

Figure A-2.—Failure surface for Black Canyon Dam core triaxial tests.
(Data compiled by Harris; data courtesy of Materials Engineering and Research Laboratory)

For any loading that is cyclic in nature, unloading/reloading data are needed to calibrate the accumulating plastic strain. The test for such data was described in section 4.0, and typical data are shown below on figure A-3.
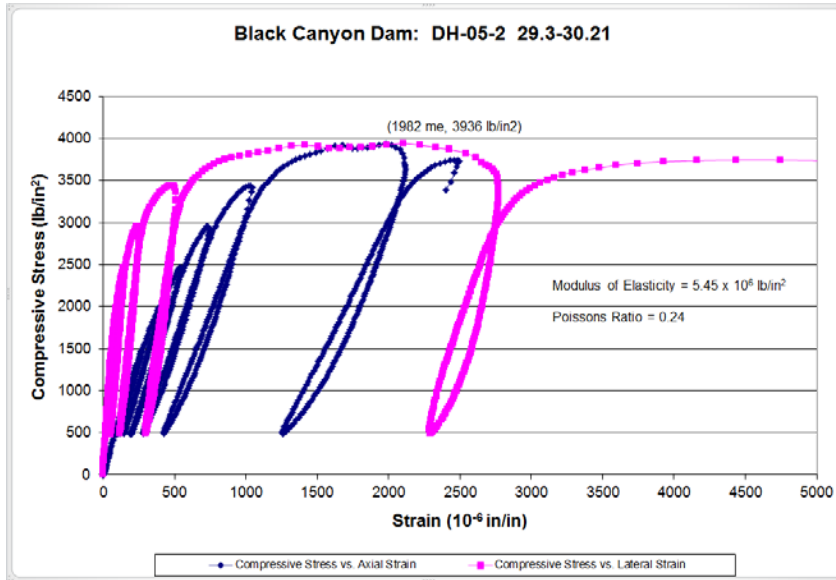

Figure A-3.—Unload/reload data for Black Canyon Dam (Madera, 2005).

Some analyses for dams consider kinematic behavior using joints rather than material analyses using plasticity-based models. Some lift joint data for Black Canyon Dam are shown below for interest.
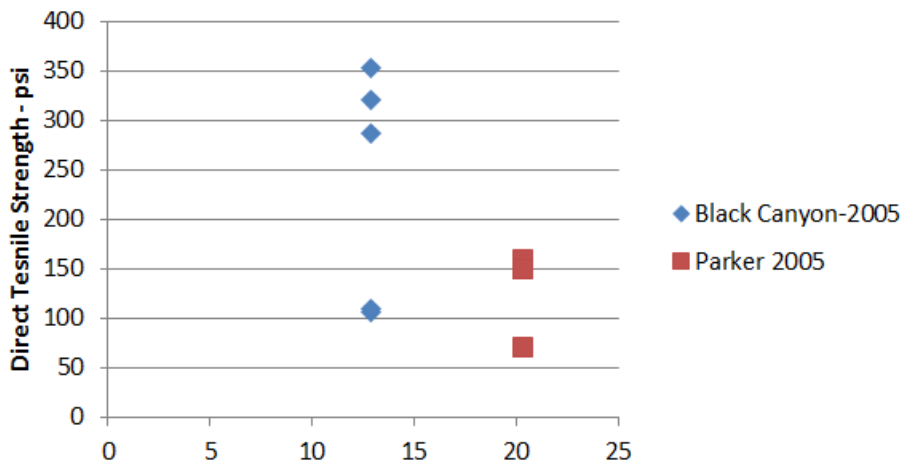

Figure A-4.—Direct tension strength of dam lift joints.
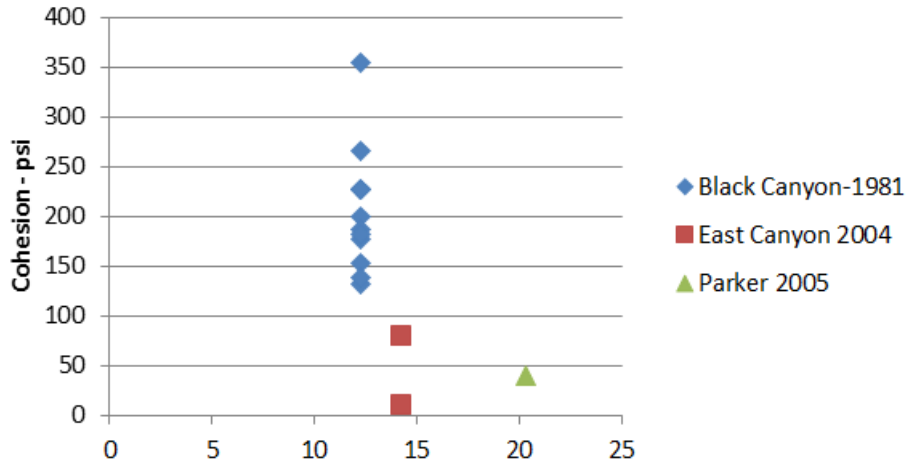(Data compiled by Harris; data courtesy of Materials Engineering and Research Laboratory).

Figure A-5.—Cohesion on dam joints tested in sliding.
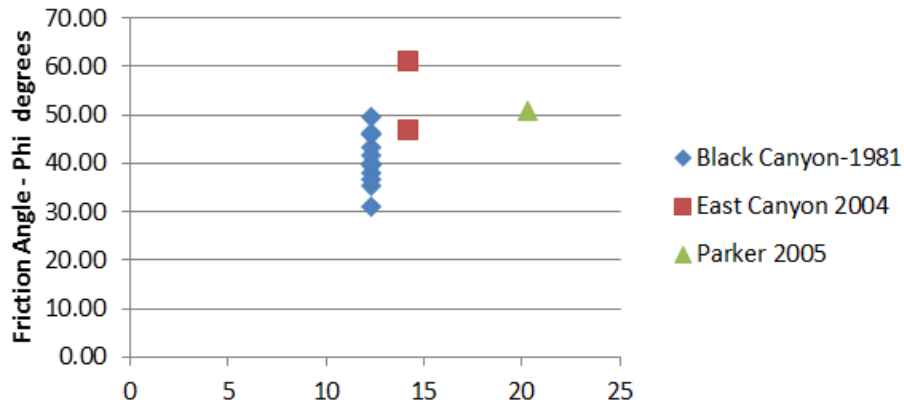(Data compiled by Harris; data courtesy of Materials Engineering and Research Laboratory).

Figure A-6.—Friction coefficient of dam joints tested in sliding.
(Data compiled by Harris; data courtesy of Materials Engineering and Research Laboratory)

ATTACHMENT B

Continuous Surface Cap Model Input Parameters

Variable	Description
G	shear modulus
K	bulk modulus
α	TXC[1] surface constant term
θ	TXC surface linear term
λ	TXC surface nonlinear term
β	TXC surface exponent
α_1	TOR[2] surface constant term
θ_1	TOR surface linear term
λ_1	TOR surface nonlinear term
β_1	TOR surface exponent
α_2	TXE[3] surface constant term
θ_2	TXE surface linear term
λ_2	TXE surface nonlinear term
β_2	TXE surface exponent
N_H	hardening initiation
C_H	hardening rate
X_0	cap initial location
W	maximum plastic volume compaction
D_1	linear shape parameter
D_2	quadratic shape parameter
B	ductile shape softening parameter
G_{fc}	fracture energy in uniaxial stress
D	Brittle shape softening parameter
G_{ft}	fracture energy in uniaxial tension
G_{fs}	fracture energy in pure shear stress
$pwrc$	shear-to-compression transition parameter
$pwrt$	shear-to-tension transition parameter
$pmod$	modify moderate pressure softening parameter
η_{0c}	rate effects parameter for uniaxial compressive stress
N_C	rate effects power for uniaxial compressive stress
η_{0t}	rate effects parameter for uniaxial tensile stress
N_t	rate effects power for uniaxial tensile stress
$Overc$	maximum overstress allowed in compression
$Overt$	maximum overstress allowed in tension
$Srate$	ratio of effective shear stress to tensile stress fluidity parameters
$Repow$	power that increases fracture energy with rate effects

---

[1] TXC = triaxial compression.
[2] TOR = triaxial torsion.
[3] TXE = triaxial extension.